Table 1 IFN-α, BUN, TP, AST, ALT, WBC, and Plt levels in mouse serum after intravenous injection of 2mg/kg apoB-1 Toc-siRNA or maltose

Treatment		IFN-α (pg/ml)	BUN (mg/dl)	TP (g/dl)	AST (U/l)	ALT (U/l)	WBC (/μl)	Plt (×10⁴/μl)
apoB-1 Toc-siRNA	3 hours	<12.5						
	24 hours		19.1 ± 1.0	5.1 ± 0.1	78 ± 1	21 ± 3	2,800 ± 330	122.0 ± 0.3
	48 hours		24.0 ± 2.4	5.5 ± 0.1	67 ± 4	22 ± 1	2,600 ± 550	112.2 ± 18.9
maltose	3 hours	<12.5						
	24 hours		22.0 ± 0.9	5.5 ± 0.1	79 ± 9	25 ± 2	2,600 ± 560	117.9 ± 13.8
	48 hours		24.5 ± 1.5	5.5 ± 0.1	60 ± 3	26 ± 3	3,700 ± 900	109.0 ± 7.0

Abbreviations: ALT, alanine aminotransferase; AST, aspartate aminotransferase; BUN, blood urea nitrogen; IFN-α, interferon-α; Plt, platelet; TP, total protein; WBC, white blood cell.
The values shown are mean values ± SEM (n = 3).

α-tocopherol did not interfere with the siRNA activity *in vitro* (**Figure 2b**).

This study showed that the binding of α-tocopherol to siRNA enables the efficient *in vivo* delivery of siRNA to the liver. The direct conjugation to siRNA of another lipophilic molecule, cholesterol (Chol-siRNA), was also reported to enhance liver uptake of siRNA.[16] However, the silencing effect produced by Toc-siRNA was more efficient than that by Chol-siRNA, in relation to the identical target gene; much higher doses of Chol-siRNA (50–100 mg/kg) were required for achieving an efficient reduction of *apoB* mRNA in the liver.[4,16] Actually, when cholesterol was conjugated to the same 27/29-mer apoB-1 siRNA with the same chemical modifications as used in apoB-1 Toc-siRNA at the 3′-end of the sense strand, the reduction of *apoB* mRNA induced by 2 mg/kg of this Chol-siRNA was not statistically significant in the livers of mice (data not shown).

The mechanism of uptake of Toc-siRNA by the liver was not elucidated, and the cause of the difference in silencing efficiency between Toc-siRNA and Chol-siRNA is not known. However, there are some possible explanations. First, if α-tocopherol and cholesterol fuse into the lipid bilayer of hepatocyte membrane as cationic liposome does, the difference in hydrophobicity and polarity between α-tocopherol and cholesterol might influence the efficiency of uptake of siRNA by the liver. This cannot be proved, however, because the negative charge of siRNA cannot be cancelled by the addition of α-tocopherol or cholesterol. Moreover, our *in vitro* experiments indicated that Toc-siRNA does not enter the hepatoma culture cell without serum. Second, Toc-siRNA might be incorporated into the serum lipoproteins and enter the hepatocytes via lipoprotein receptors. Recently, Chol-siRNA was shown to use the lipoprotein receptor–mediated pathway to enter hepatocytes.[23] In contrast to cholesterol, α-tocopherol is an exogenous lipid which cannot be synthesized *in vivo*, and therefore the distribution of α-tocopherol among lipoproteins and the mediating receptors in the liver might be different from those of cholesterol. Third, binding of α-tocopherol might enhance uptake of siRNA in the liver by an interacting serum molecule other than lipoprotein. Soutschek and colleagues[16] proposed that the mechanism of Chol-siRNA *in vivo* is related to enhanced binding to serum protein such as albumin. Similarly, α-tocopherol is known to interact with other serum proteins such as SEC14L2, SEC14L3, SEC14L4, and afamin (reviewed in ref. 14).

We observed significant decreases of serum TG and cholesterol and an increase in lipid droplets in the liver after injection of apoB-1 Toc-siRNA. The downregulation of liver ApoB-100 impairs VLDL export and is expected to decrease serum TG as well as cholesterol, because large amounts of TG are incorporated into VLDL particles. This is supported by the fact that the transgenic mouse of truncated *apoB*,[24] and the microsomal TG transfer protein-null mouse,[25,26] neither of which can assemble and secrete VLDL in the liver, show lower serum TG and cholesterol and an accumulation of lipid droplets in the liver. Our results, showing decrease in serum TG as well as in cholesterol, were similar to those of a recent study that used a different siRNA *in vivo* delivery system.[8] Although the decreases in serum TG and cholesterol might be caused by mechanisms other than impaired VLDL export, these results indicate the phenotype of ApoB-100 silencing by Toc-siRNA.

There was no remarkable side effect in blood cell count and biochemical analysis after intravenous injection of Toc-siRNA. The delivered amount of α-tocopherol was only 46 μg/kg when 2 mg/kg Toc-siRNA was injected. This value is very small, considering the need of α-tocopherol as a nutritional element is estimated 10 mg/day for man (125–200 μg/kg/day).[27] In addition, the anti-oxidant activity of α-tocopherol in Toc-siRNA is abolished, because the reactive site of α-tocopherol for anti-oxidation, hydroxyl group at the C6 position, is covalently connected to siRNA (**Figure 1a**). More important, the Toc-siRNA did not induce IFN-α in serum (**Table 1**) and *IFN-β* mRNA in the liver. This absence of adverse side effects associated with the use of Toc-siRNA is important to note, because it is in sharp contrast to the outcome generally described for lipid vector–associated siRNA delivery. The latter is known to produce an immunostimulatory effect,[28] which could cause elevation of transaminases, thrombocytopenia, and lymphopenia.[29] When synthetic lipid-coated siRNA is intravenously injected, it is incorporated in the endosome and then induces IFNs and cytokines through activation of Toll-like receptors located in the endosomal membrane.[20] The possible mechanism of escape from an immunostimulatory effect in Toc-siRNA-injected mice was that Toc-siRNA used the different pathway to enter the cells from synthetic lipid-coated siRNAs. Together, Toc-siRNA is considered to be a noninvasive delivery method of siRNA.

In summary, vitamin E–mediated *in vivo* delivery of siRNA is effective and safe. Although further investigation into the precise delivery pathway of Toc-siRNA is required for better optimization of its use, the findings of this study represent an important step in advancing the use of synthetic siRNA as a very promising system for gene therapy.

MATERIALS AND METHODS

Synthesis of siRNAs. siRNAs were chemically synthesized. In order to combine vitamin E with siRNA, α-tocopherol phosphoramidite was prepared, and then was it connected with the 5′-end of the antisense strand of the siRNA. The DL-α-tocopherol was purchased from Tokyo Kasei, Tokyo, Japan. Synthetic sense and antisense strands of siRNA were then annealed.

Cell culture. Hepa 1-6 cells were maintained in Dulbecco's modified Eagle's medium (Sigma-Aldrich, St Louis, MO) only, or supplemented with 10% fetal bovine serum (Invitrogen, Carlsbad, CA), 100 U/ml penicillin, and 100 μg of streptomycin at 37 °C in 5% CO_2.

qRT-PCR. Total RNA was extracted from the culture cells or mice liver using Isogen (Nippon Gene, Tokyo, Japan). The RNA was reverse transcribed with Superscript III and random hexamers (Invitrogen, Carlsbad, CA). The qRT-PCR was performed on 1.5 μg of complementary DNA using the TaqMan Universal PCR Master Mix (Applied Biosystems, Foster City, CA) in accordance with the manufacturer's instructions. The amplification conditions were 40 cycles of denaturation at 95 °C for 15 seconds and annealing at 60 °C for 60 seconds with ABI PRISM 7700 Sequence Detector. Primers for mouse *apoB*, *gapdh*, *ttr*, and *IFN-β* mRNAs were designed by Applied Biosystems (Foster City, CA).

In vitro *activity and stability assays.* In order to determine *in vitro* activity of siRNAs, Hepa 1-6 cells were transfected with 10 nmol/l of siRNAs using Lipofectamine RNAiMAX (Invitrogen, Carlsbad, CA), or transfected with 2 μmol/l of Toc-siRNAs without any transfection reagents. The cells were harvested 24 hours after transfection. Total RNA was extracted and the amount of endogenous *apoB* mRNA was measured using qRT-PCR.

In order to study the stability of the siRNAs in serum, (i) siRNA with both strands naked, (ii) siRNA with both strands modified, (iii) siRNA with only the sense strand modified, (iv) Toc-siRNA with both strands naked, and (v) Toc-siRNA with both strands modified (100 pmol each) were incubated at 37 °C in mouse serum for 4, 8, 16, and 24 hours. Aliquots taken at different time points were treated with Proteinase K (Wako Pure Chemical Industries, Osaka, Japan) and frozen in urea Tris-buffered electrophoresis-loading buffer. All samples were subjected to electrophoresis on 2% agarose gels.

Northern blotting. Total RNA was extracted from mice liver using MirVana (Ambion, Austin, TX). Total RNA was condensed with Ethachinmate (Nippon gene) and 2 μg of RNA was separated by electrophoresis on a 14% polyacrylamide-urea gel and transferred to a Hybond-N^+ membrane (Amersham Biosciences, Piscataway, NJ). The blot was hybridized with a probe of the siRNA antisense sequence which was labeled with fluorescein using Gene Images 3′-Oligolabelling kit (Amersham Biosciences, Piscataway, NJ). The signals were visualized by Gene Images CDP-star detection Kit (Amersham Biosciences, Piscataway, NJ).

Pathological analysis. For pathological analysis of side effects by Toc-siRNA, the liver sample was postfixed in 4% paraformaldehyde/phosphate-buffered saline solution for 6 hour and embedded in paraffin, sectioned at 4-μm thick using a Leica CM 3050 S cryostat (Leica Microsystems, Wetzlar, Germany), and then stained with hematoxylin/eosin.

To analyze of liver lipid accumulation, liver samples from apoB-1 and control Toc-siRNA-treated mice were sectioned (4 μm) and fixed in 4% paraformaldehyde/phosphate-buffered saline for 5 minutes, and then stained with filtrated Sudan III (Muto Pure Chemicals, Tokyo, Japan) 37 °C for 30 minutes. Counterstaining of nuclei was performed with Mayer hematoxylin solution (Muto Pure Chemicals, Tokyo, Japan) for 3 minutes.

For pathological analysis of delivery of siRNA to liver, 8 mg/kg Cy3-labeled siRNA with or without α-tocopherol within 0.25 ml of 10% maltose was injected from the tail vein of ICR mouse. One hour after intravenous injection, mouse was killed and liver samples were harvested. Liver samples were fixed in 4% paraformaldehyde/phosphate-buffered saline for 6 hour. Fixed tissue samples were snap-frozen in liquid nitrogen. Frozen tissue sections were prepared and stained with 13 nmol/l Alexa-488 phalloidin (Invitrogen, Carlsbad, CA). The slides were analyzed using LSM 510 confocal microscope (Carl Zeiss MicroImaging, Oberkochen, Germany). Each image comprised a flattened projection of 11 optical images (0.4 μm each) to represent combined fluorescence signals from a 4-μm thick section.

Statistical analysis. Student's *t*-test was used to evaluate differences between siRNA-transfected groups and cells alone *in vitro*, and between Toc-siRNA-injected groups and maltose only injected group *in vivo*.

ACKNOWLEDGMENTS

We thank Tadaaki Ohgi, Nippon Shinyaku, for his technical support. This work was supported by grants from the Ministry of Education, Science and Culture, Japan (#18650103) and the Ministry of Health Labor and Welfare, Japan (#2212065), and a grant from the 21st Century Center of Excellence Program on Brain Integration and its Disorders given to Tokyo Medical and Dental University.

REFERENCES

1. Davidson, BL and Harper, SQ (2005). Viral delivery of recombinant short hairpin RNAs. *Methods Enzymol* **392**: 145–173.
2. McCaffrey, AP, Meuse, L, Pham, TT, Conklin, DS, Hannon, GJ and Kay, MA (2002). RNA interference in adult mice. *Nature* **418**: 38–39.
3. Hino, T, Yokota, T, Ito, S, Nishina, K, Kang, YS, Mori, S *et al.* (2006). *In vivo* delivery of small interfering RNA targeting brain capillary endothelial cells. *Biochem Biophys Res Commun* **340**: 263–267.
4. Zimmermann, TS, Lee, AC, Akinc, A, Bramlage, B, Bumcrot, D, Fedoruk, MN *et al.* (2006). RNAi-mediated gene silencing in non-human primates. *Nature* **441**: 111–114.
5. Yokota, T, Iijima, S, Kubodera, T, Ishii, K, Katakai, Y, Ageyama, N *et al.* (2007). Efficient regulation of viral replication by siRNA in a non-human primate surrogate model for hepatitis C. *Biochem Biophys Res Commun* **361**: 294–300.
6. Spagnou, S, Miller, AD and Keller, M (2004). Lipidic carriers of siRNA: differences in the formulation, cellular uptake, and delivery with plasmid DNA. *Biochemistry* **43**: 13348–13356.
7. Baigude, H, McCarroll, J, Yang, CS, Swain, PM and Rana, TM (2007). Design and creation of new nanomaterials for therapeutic RNAi. *ACS Chem Biol* **2**: 237–241.
8. Rozema, DB, Lewis, DL, Wakefield, DH, Wong, SC, Klein, JJ, Roesch, PL *et al.* (2007). Dynamic PolyConjugates for targeted *in vivo* delivery of siRNA to hepatocytes. *Proc Natl Acad Sci USA* **104**: 12982–12987.
9. Sato, A, Takagi, M, Shimamoto, A, Kawakami, S and Hashida, M (2007). Small interfering RNA delivery to the liver by intravenous administration of galactosylated cationic liposomes in mice. *Biomaterials* **28**: 1434–1442.
10. Kim, SI, Shin, D, Choi, TH, Lee, JC, Cheon, GJ, Kim, KY *et al.* (2007). Systemic and specific delivery of small interfering RNAs to the liver mediated by apolipoprotein A-I. *Mol Ther* **15**: 1145–1152.
11. Kumar, P, Wu, H, McBride, JL, Jung, KE, Kim, MH, Davidson, BL *et al.* (2007). Transvascular delivery of small interfering RNA to the central nervous system. *Nature* **448**: 39–43.
12. Kappus, H and Diplock, AT (1992). Tolerance and safety of vitamin E: a toxicological position report. *Free Radic Biol Med* **13**: 55–74.
13. Rigotti, A (2007). Absorption, transport, and tissue delivery of vitamin E. *Mol Aspects Med* **28**: 423–436.
14. Zingg, JM (2007). Vitamin E: an overwiew of major research directions. *Mol Aspects Med* **28**: 400–422.
15. Rose, SD, Kim, DH, Amarzguioui, M, Heidel, JD, Collingwood, MA, Davis, ME *et al.* (2005). Functional polarity is introduced by Dicer processing of short substrate RNAs. *Nucleic Acids Res* **33**: 4140–4156.
16. Soutschek, J, Akinc, A, Bramlage, B, Charisse, K, Constien, R, Donoghue, M *et al.* (2004). Therapeutic silencing of an endogenous gene by systemic administration of modified siRNAs. *Nature* **432**: 173–178.
17. Chiu, YL and Rana, TM (2003). siRNA function in RNAi: a chemical modification analysis. *RNA* **9**: 1034–1048.
18. Czauderna, F, Fechtner, M, Dames, S, Aygün, H, Klippel, A, Pronk, GJ *et al.* (2003). Structural variations and stabilising modifications of synthetic siRNAs in mammalian cells. *Nucleic Acids Res* **31**: 2705–2716.
19. Miyoshi, K, Tsukumo, H, Nagami, T, Siomi, H and Siomi, MC (2005). Slicer function of *Drosophila* Argonautes and its involvement in RISC formation. *Genes Dev* **19**: 2837–2848.
20. Judge, AD, Bola, G, Lee, AC and MacLachlan, I (2006). Design of noninflammatory synthetic siRNA mediating potent gene silencing *in vivo*. *Mol Ther* **13**: 494–505.
21. Sioud, M, Furset, G and Cekaite, L (2007). Suppression of immunostimulatory siRNA-driven innate immune activation by 2′-modified RNAs. *Biochem Biophys Res Commun* **361**: 122–126.

22. Altergood, L and Alfin-Slater, RB (1978). Effect of administration of α- and γ-tocopherol on tissue distribution and red cell hemolysis in rats. *Int J Vitam Nutr Res* **48**: 32–37.
23. Wolfrum, C, Shi, S, Jayaprakash, KN, Jayaraman, M, Wang, G, Pandey, RK *et al.* (2007). Mechanisms and optimization of *in vivo* delivery of lipophilic siRNAs. *Nat Biotechnol* **25**: 1149–1157.
24. Chen, Z, Fitzgerald, RL, Averna, MR and Schonfeld, G (2000). A targeted apolipoprotein B-38.9-producing mutation causes fatty livers in mice due to the reduced ability of apolipoprotein B-38.9 to transport triglycerides. *J Biol Chem* **275**: 32807–32815.
25. Raabe, M, Véniant, MM, Sullivan, MA, Zlot, CH, Björkegren, J, Nielsen, LB *et al.* (1999). Analysis of the role of microsomal triglyceride transfer protein in the liver of tissue-specific knockout mice. *J Clin Invest* **103**: 1287–1298.
26. Minehira-Castelli, K, Leonard, SW, Walker, QM, Traber, MG and Young, SG (2006). Absence of VLDL secretion does not affect α-tocopherol content in peripheral tissues. *J Lipid Res* **47**: 1733–1738.
27. Food and Nutrition Board, National Academy of Sciences, National Research Council (1989). *Recommended Dietary Allowances* 10th edn. National Academy Press: Washington, DC, pp 99–107.
28. Robbins, M, Judge, A, Liang, L, McClintock, K, Yaworski, E and MacLachlan, I (2007). 2'-O-methyl-modified RNAs act as TLR7 antagonists. *Mol Ther* **15**: 1663–1669.
29. Morrissey, DV, Lockridge, JA, Shaw, L, Blanchard, K, Jensen, K, Breen, W *et al.* (2005). Potent and persistent *in vivo* anti-HBV activity of chemically modified siRNAs. *Nat Biotechnol* **23**: 1002–1007.

doi:10.1111/j.1440-1746.2007.05076.x

HEPATOLOGY

Inhibition of hepatitis C virus infection and expression *in vitro* and *in vivo* by recombinant adenovirus expressing short hairpin RNA

Naoya Sakamoto,*,† Yoko Tanabe,* Takanori Yokota,‡ Kenichi Satoh,§ Yuko Sekine-Osajima,* Mina Nakagawa,*,† Yasuhiro Itsui,* Megumi Tasaka,* Yuki Sakurai,* Chen Cheng-Hsin,* Masahiko Yano,¶ Shogo Ohkoshi,¶ Yutaka Aoyagi,¶ Shinya Maekawa,†† Nobuyuki Enomoto,†† Michinori Kohara§ and Mamoru Watanabe*

Departments of *Gastroenterology and Hepatology, †Hepatitis Control, and ‡Neurology and Neurological Science, Tokyo Medical and Dental University, §Department of Microbiology and Cell Biology, The Tokyo Metropolitan Institute of Medical Science, Tokyo, ¶Gastroenterology and Hepatology Division, Graduate School of Medical and Dental Sciences, Niigata University, Niigata, and ††First Department of Medicine, Yamanashi University, Yamanashi, Japan

Key words
adenovirus vector, hepatitis C virus, RNA interference.

Accepted for publication 12 April 2007.

Correspondence
Dr Naoya Sakamoto, Department of Gastroenterology and Hepatology, Tokyo Medical and Dental University, 1-5-45 Yushima, Bunkyo-ku, Tokyo 113-8519, Japan.
Email: nsakamoto.gast@tmd.ac.jp

NS and YT have contributed equally to this paper.

Abstract

Background and Aim: We have reported previously that synthetic small interfering RNA (siRNA) and DNA-based siRNA expression vectors efficiently and specifically suppress hepatitis C virus (HCV) replication *in vitro*. In this study, we investigated the effects of the siRNA targeting HCV-RNA *in vivo*.

Methods: We constructed recombinant retrovirus and adenovirus expressing short hairpin RNA (shRNA), and transfected into replicon-expressing cells *in vitro* and transgenic mice *in vivo*.

Results: Retroviral transduction of Huh7 cells to express shRNA and subsequent transfection of an HCV replicon into the cells showed that the cells had acquired resistance to HCV replication. Infection of cells expressing the HCV replicon with an adenovirus expressing shRNA resulted in efficient vector delivery and expression of shRNA, leading to suppression of the replicon in the cells by ~10^{-3}. Intravenous delivery of the adenovirus expressing shRNA into transgenic mice that can be induced to express HCV structural proteins by the Cre/*lox*P switching system resulted in specific suppression of virus protein synthesis in the liver.

Conclusion: Taken together, our results support the feasibility of utilizing gene targeting therapy based on siRNA and/or shRNA expression to counteract HCV replication, which might prove valuable in the treatment of hepatitis C.

Introduction

Hepatitis C virus (HCV), which affects 170 million people worldwide, is one of the most important pathogens causing liver-related morbidity and mortality.[1] The difficulty in eradicating HCV is attributable to limited treatment options against the virus and their unsatisfactory efficacies. Even with the most effective regimen with pegylated interferon (IFN) and ribavirin in combination, the efficacies are limited to less than half of the patients treated.[2] Given this situation, the development of safe and effective anti-HCV therapies is one of our high-priority goals.

RNA interference (RNAi) is a process of sequence-specific, post-transcriptional gene silencing that is initiated by double-stranded RNA.[3,4] Because of its potency and specificity, RNAi rapidly has become a powerful tool for basic research to analyze gene functions and for potential therapeutic applications. Recently, successful suppression of various human pathogens by RNAi have been reported, including human immunodeficiency viruses,[5,6] poliovirus,[7] influenza virus,[8] severe acute respiratory syndrome (SARS) virus[9] and hepatitis B virus (HBV).[10–13]

We and other researchers have reported that appropriately designed small interfering RNA (siRNA) targeting HCV genomic RNA can efficiently and specifically suppress HCV replication *in vitro*.[14–19] We have tested siRNA designed to target the well-conserved 5′-untranslated region (5′-UTR) of HCV-RNA, and identified the most effective target, just upstream of the translation initiation codon. Furthermore, transfection of DNA-based vectors expressing siRNA was as effective as that of synthetic siRNA in suppressing HCV replication.[14]

In this study, we explored the further possibility that efficient delivery and expression of siRNA may be effective in suppression and elimination of HCV replication and that delivery of such

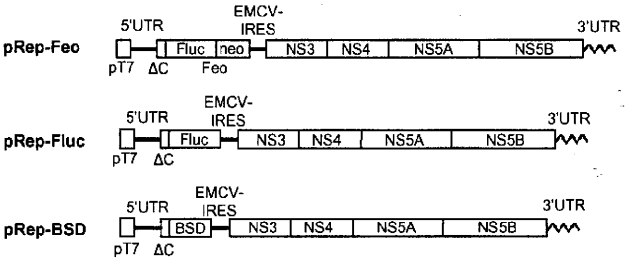

Figure 1 Structures of HCV replicon plasmids. The pRep-Feo expressed a chimeric reporter protein of firefly luciferase (Fluc) and neomycin phosphotransferase (GenBank accession No. AB119282).[14,20] The pRep-Fluc expressed the Fluc protein. The pRep-BSD expressed the blasticidin S (BSD) resistance gene. pT7, T7 promoter; 5'UTR, HCV 5'-untranslated region; ΔC, truncated HCV core region (nt. 342–377); neo, neomycin phosphotransferase gene; EMCV, encephalomyocarditis virus; NS3, NS4, NS5A and NS5B, genes that encode HCV non-structural proteins; 3'UTR, HCV 3'-untranslated region.

HCV-directed siRNA *in vivo* may be effective in silencing viral protein expression in the liver. Here, we report that HCV replication was suppressed *in vitro* by recombinant retrovirus and adenovirus vectors expressing short hairpin RNA (shRNA) and that the delivery of the adenovirus vector to mice *in vivo* specifically inhibited viral protein synthesis in the liver.

Methods

Cells and cell culture

Huh7 and Retro Pack PT67 cells (Clontech, Palo Alto, CA, USA) were maintained in Dulbecco's modified minimal essential medium (Sigma, St. Louis, MO, USA) supplemented with 10% fetal calf serum at 37°C under 5% CO_2. To maintain cell lines carrying the HCV replicon, G418 (Wako, Osaka, Japan) was added to the culture medium to a final concentration of 500 μg/mL.

HCV replicon constructs and transfection

HCV replicon plasmids, pRep-Feo, pRep-Fluc and pRep-BSD were constructed from were constructed from a virus, HCV-N strain, genotype 1b.[21] The pRep-Feo expressed a chimeric reporter protein of firefly luciferase (Fluc) and neomycin phosphotransferase.[14,20] The pRep-Fluc and the pRep-BSD expressed the Fluc and blasticidin S (BSD) resistance genes, respectively (Fig. 1). The replicon RNA synthesis and the transfection protocol have been described previously.[22]

Synthetic siRNA and siRNA-expression plasmid

The design and construction of HCV-directed siRNA vectors have been described.[14] Briefly, five siRNA targeting the 5'-UTR of HCV RNA were tested for their efficiency to inhibit HCV replication, and the most effective sequence, which targeted nucleotide position of 331 though 351, was used in the present study. To construct shRNA-expressing DNA cassettes, oligonucleotide inserts were synthesized that contained the loop sequence (5'-TTC AAG AGA-3') flanked by sense and antisense siRNA sequences (Fig. 2a). These were inserted immediately downstream of the human U6 promoter. To avoid a problem in transcribing shRNA because of instability of the DNA strands arising from the tight palindrome structure, several C-to-T point mutations, which retained completely the silencing activity of the shRNA, were introduced into the sense strand of the shRNA sequences (referred to as 'm').[23] A control plasmid, pUC19-shRNA-Control, expressed shRNA directed towards the Machado–Joseph disease gene, which is a mutant of ataxin-3 gene and is not normally expressed. We have previously described the sequence specific activity of the shRNA-Control.[24]

Prior to construction of the virus vectors, we tested silencing efficiency of five shRNA constructs of different lengths that covered the target sequence (Fig. 2a). The shRNA-HCV-19, shRNA-HCV-21 and shRNA-HCV-27 had target sequences of 19, 21 and 27 nucleotides, respectively. Transfection of these shRNA constructs into Huh7/pRep-Feo showed that shRNA with longer target sequences had better suppressive effects (Fig. 2b). Therefore, we used shRNA-HCV-27m (abbreviated as shRNA-HCV) in the following study.

Recombinant retrovirus vectors

The U6-shRNA expression cassettes were inserted into the *StuI*/*Hin*dIII site of a retrovirus vector, pLNCX2 (Clontech) to construct pLNCshRNA-HCV and pLNCshRNA-Control (Fig. 2c). The plasmids were transfected into the packaging cells, Retro Pack PT67. The culture supernatant was filtered and added onto Huh7 cells with 4 μg/mL of polybrene. Huh7 cell lines stably expressing shRNA were established by culture in the presence of 500 μg/mL of G418.

Recombinant adenovirus

Recombinant adenoviruses expressing shRNA were constructed using an Adenovirus Expression Vector Kit (Takara, Otsu, Japan). The U6-shRNA expression DNA cassette was inserted into the *Swa*I site of pAxcw to construct pAxshRNA-HCV and pAxshRNA-Control. The adenoviruses were propagated according to the manufacturer's protocol (AxshRNA-HCV and AxshRNA-Control; Fig. 2c). A 'multiplicity of infection' (MOI) was used to standardize infecting doses of adenovirus. The MOI stands for the ratio of infectious virus particles to the number of cells being infected. An MOI = 1 represents equivalent dose to introduce one infectious virus particle to every host cell that is present in the culture.

Plasmids for assays of interferon responses

pISRE-TA-Luc (Invitrogen, Carlsbad, CA, USA) contained five copies of the consensus interferon stimulated response element (ISRE) motifs upstream of the Fluc gene. pTA-Luc (Invitrogen), which lacks the enhancer element, was used for background determination. The pcDNA3.1 (Invitrogen) was used as an empty vector for mock transfection. pRL-CMV (Promega, Madison, WI, USA), which expresses the *Renilla* luciferase protein, was used for normalization of transfection efficiency.[25] A plasmid, peGFPneo (Invitrogen), was used to monitor percentages of transduced cells.

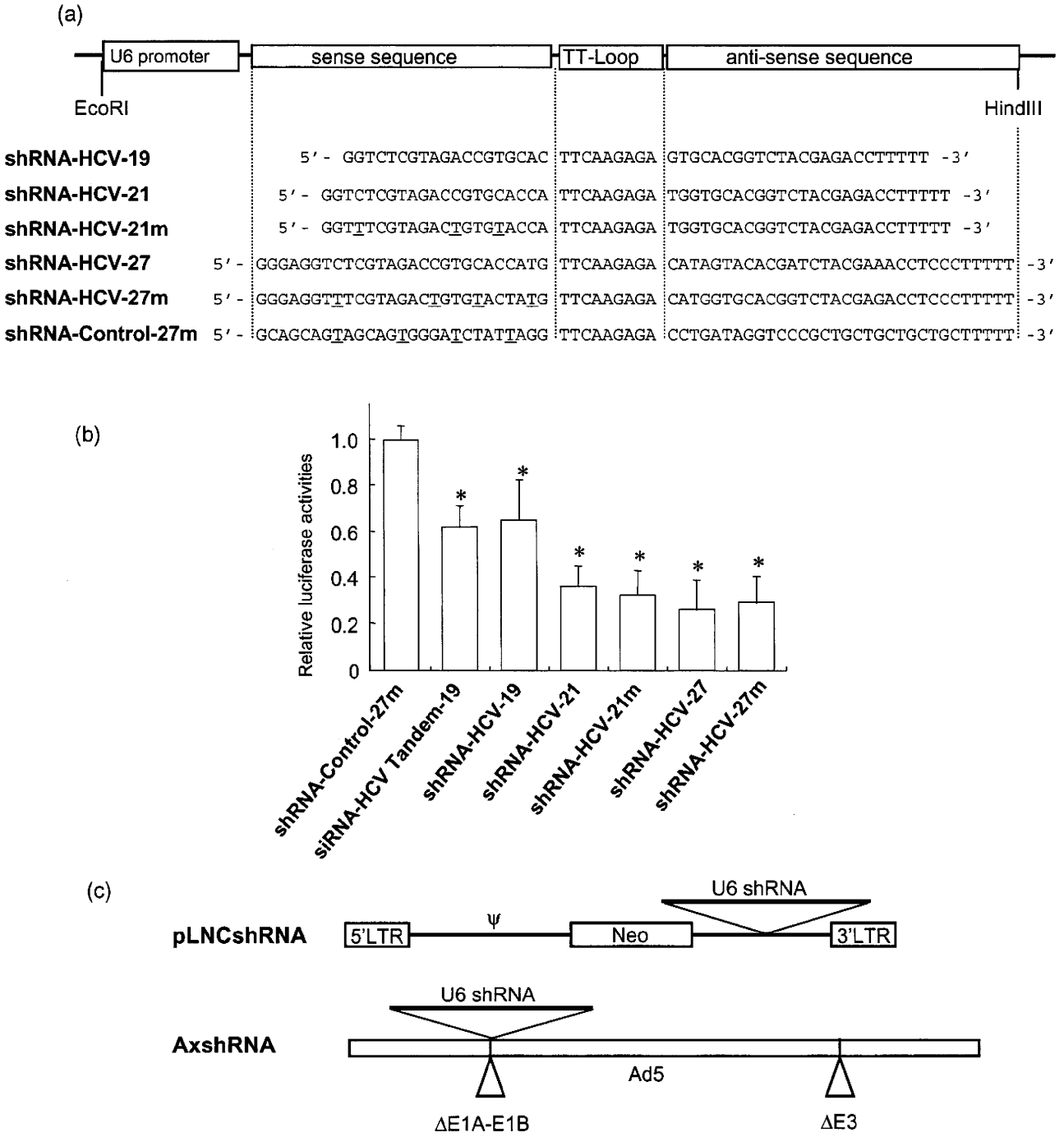

Figure 2 Structure of shRNA-expression constructs and shRNA sequences. (a) Structure of shRNA-expression cassette and shRNA sequences. TT-Loop, the loop sequence. The shRNA-Control was directed toward an unrelated target, Machado–Joseph disease gene. Underlined letters indicate C-to-T point mutations in the sense strand. (b) The shRNA-expression plasmids were transfected into Huh7/pRep-Feo cells, and internal luciferase activities were measured at 48 h of transfection. Each assay was done in triplicate, and the values are displayed as mean + SD. $*P < 0.05$. (c) pLNCshRNA, structure of a recombinant retrovirus expressing shRNA. Ψ, the retroviral packaging signal sequence. AxshRNA, structure of a recombinant adenovirus expressing shRNA.

Real-time RT-PCR analysis

Total cellular RNA was extracted from cultured cells or liver tissue using ISOGEN (Nippon Gene, Tokyo, Japan). Total cellular RNA (2 μg) was used to generate cDNA from each sample using the SuperScript II reverse-transcriptase (Invitrogen). The mRNA expression levels were measured using the Light Cycler PCR and detection system (Roche, Mannheim, Germany) and Light Cycler Fast Start DNA Master SYBR Green 1 mix (Roche).

Luciferase assays

Luciferase activity was measured using a luminometer, Lumat LB9501 (Promega) and the Bright-Glo Luciferase Assay System (Promega) or the Dual-Luciferase Reporter Assay System (Promega).

Northern and western hybridization

Total cellular RNA was separated by denaturing agarose-formaldehyde gel electrophoresis, and transferred to a nylon membrane. The membrane was hybridized with a digoxigenin-labeled probe specific for the full-length replicon sequence, and subsequently with a probe specific for beta-actin. The signals were detected by chemiluminescence reaction using a Digoxigenin Luminescent Detection Kit (Roche), and visualized by Fluoro-Imager (Roche). For the western blotting, 10 μg of total cell lysate was separated on NuPAGE 4.12% Bis-TrisGel (Invitrogen), and blotted onto an Immobilon PVDF Membrane (Roche). The membrane was incubated with monoclonal antibodies specific for HCV-NS5A (BioDesign, Saco, ME, USA), NS4A (Virogen, Watertown, MA, USA), or beta-actin (Sigma), and detected by a chemiluminescence reaction (BM Chemiluminescence Blotting Substrate; POD, Roche).

Transient-replication assays

A replicon, pRep-Fluc, was transfected into cells and the luciferase activities of the cell lysates were measured serially. To correct the transfection efficiency, each value was divided by the luciferase activity at 4 h after the transfection.

Stable colony formation assays

Cells were transfected with a replicon, pRep-BSD, and were cultured in the presence of 150 μg/mL of BSD (Invitrogen). BSD-resistant cell colonies appeared after ~3 weeks of culture, and were counted.

HCV-JFH1 virus cell culture

An *in-vitro* transcribed HCV-JFH1 RNA[26] was transfected into Huh7.5.1 cells.[27] Naive Huh7.5.1 cells were subsequently infected by the culture supernatant of the JFH1-RNA transfected Huh-7.5.1 cells, and subjected to siRNA or drug treatments. Replication levels of HCV-RNA were quantified by the realtime RT-PCR by using primers that targeted HCV-NS5B region, HCV-JFH1 sense: 5′-TCA GAC AGA GCC TGA GTC CA-3′, and HCV-JFH1 antisense: 5′-AGT TGC TGG AGG GCT TCT GA-3′.

Mice and adenovirus infection

Transgenic mice, CN2-29, inducibly express mRNA for the HCV structural proteins (genotype1b, nucleotides 294–3435) by the Cre/*lox*P switching system.[28] The transgene does not contain full-length HCV 5′-UTR, but shares the target sequence of the shRNA-HCV. Although the transgenic mouse CN2 has been previously reported as expressing higher levels of the viral proteins, the expression levels of the viral core protein in the CN2-29 mice are modest and similar to that in the liver of HCV patients. Thus, we chose CN2-29 mice in the present study.

The mice were infected with AxshRNA-HCV or controls (AxshRNA-Control or AxCAw1) in combination with AxCAN-Cre, which expressed Cre recombinase. Three days after the infection, the mice were killed and HCV core protein in the liver was measured as described below. The BALB/c mice were maintained in the Animal Care Facility of Tokyo Medial and Dental University, and transgenic mice were in the Tokyo Metropolitan Institute of Medical Science. Animal care was in accordance with institutional guidelines. The review board of the university approved our experimental animal studies and all experiments were approved by the institutional animal study committees.

Measurement of HCV core protein in mouse liver

The amounts of HCV core protein in the liver tissue from the mice was measured by a fluorescence enzyme immunoassay (FEIA)[29] with a slight modification. Briefly, the 5F11 monoclonal anti-HCV-core antibody was used as the first antibody on the solid phase, and the 5E3 antibody conjugated with horseradish peroxidase was the second antibody. This FEIA can detect as little as 4 pg/mL of recombinant HCV-core protein. Contents of the HCV core protein in the liver samples were normalized by the total protein contents and expressed as pg/mg total protein.

Immunohistochemical staining

Liver tissue was frozen with optimal cutting temperature (OTC) compound (Tissue Tek; Sakura Finetechnical, Tokyo, Japan). The sections (8 μm thick) were fixed with a 1:1 solution of acetone : methanol at −20°C for 10 min and then washed with phosphate-buffered saline (PBS). Subsequently, the sections were incubated with the IgG fraction of an anti-HCV core rabbit polyclonal antibody (RR8)[28] in blocking buffer or antialbumin rabbit polyclonal antibody (Dako Cytomation, Glostrup, Denmark) in PBS overnight at 4°C. The sections were incubated with secondary antibody, Alexa-antirabbit IgG (Invitrogen) or TRITIC-antirabbit IgG (Sigma), for 2 h at room temperature. Fluorescence was observed using a fluorescence microscope.

Statistical analyses

Statistical analyses were performed using Student's *t*-test; *P*-values of less than 0.05 were considered to be statistically significant.

Results

Retrovirus transduction of shRNA can protect from HCV replication

Retrovirus vectors propagated from pLNCshRNA-HCV and pLNCshRNA-Control were used to infect Huh7 cells, and cell lines were established that constitutively express shRNA-HCV and shRNA-Control (Huh7/shRNA-HCV and Huh7/shRNA-Control, respectively). There were no differences in the cell morphology or growth rate between shRNA-transduced and non-transduced Huh7 cells (data not shown). The HCV replicon, pRep-Fluc, was transfected into Huh7/shRNA-HCV, Huh7/shRNA-Control and naive Huh7 cells by electroporation. In Huh7/shRNA-Control and naive Huh7 cells, the initial luciferase activity at 4 h decreased temporarily, which represents decay of the transfected replicon RNA, but increased again at 48 h and 72 h, which demonstrate de novo synthesis of the HCV replicon RNA. In contrast, transfection into Huh7/shRNA-HCV cells resulted in a decrease in the initial luciferase activity, reaching background by 72 h (Fig. 3a). Similarly, transfection of the replicon, pRep-BSD, into Huh7 cells and BSD selection yielded numerous BSD-resistant colonies in the naive Huh7 (832 colonies) and Huh7/shRNA-Control cell lines (740 colonies), while transfection of Huh7/shRNA-HCV, which expressed shRNA-HCV, yielded obviously fewer colonies (five colonies), indicating reduction of colony forming units by ~10^2 (Fig. 3b). There was no difference in shape, growth or viability between cells expressing the shRNA or not. These results indicated that cells expressing HCV-directed shRNA following retrovirus transduction acquired resistance to HCV replication.

Effect of recombinant adenoviruses expressing shRNA on *in vitro* HCV replication

We investigated subsequently the effects of recombinant adenovirus vectors expressing shRNA. AxshRNA-HCV and AxshRNA-Control were used separately to infect Huh7/pRep-Feo cells, and the internal luciferase activities were measured sequentially (Fig. 4a). AxshRNA-HCV caused continuous suppression of HCV RNA replication. Six days postinfection, the luciferase activities fell to background levels. In contrast, the luciferase activities of the Huh7/pRep-Feo cells infected with AxshRNA-Control did not show any significant changes compared with untreated Huh7/pRep-Feo cells (Fig. 4a). The dimethylthiazol carboxymethoxyphenyl sulfophenyl tetrazolium (MTS) assay showed no significant difference between cells that were infected by recombinant adenovirus and uninfected cells (Fig. 4b). In the northern blotting analysis, the cells were harvested 6 days after infection with the adenovirus at an MOI of 1. Feo-replicon RNA of 9.6 kb, which was detectable in the untreated Huh7/pRep-Feo cells and in the cells infected with AxshRNA-Control, diminished substantially following infection with the AxshRNA-HCV (Fig. 4c). Densitometries showed that the intracellular levels of the replicon RNA in the Huh7/pRep-Feo cells correlated well with the internal luciferase activities. Similarly in the western blotting, cells were harvested 6 days after infection with adenovirus. Levels of the HCV NS4A and NS5A proteins that were translated from the HCV replicon decreased following infection with the AxshRNA-HCV (Fig. 4d). These results indicated that the decrease in luciferase activities was due to specific suppressive effects of shRNA on expression of HCV genomic RNA and the viral proteins, and not due to non-specific effects caused by the delivery of shRNA or to toxicity of the adenovirus vectors.

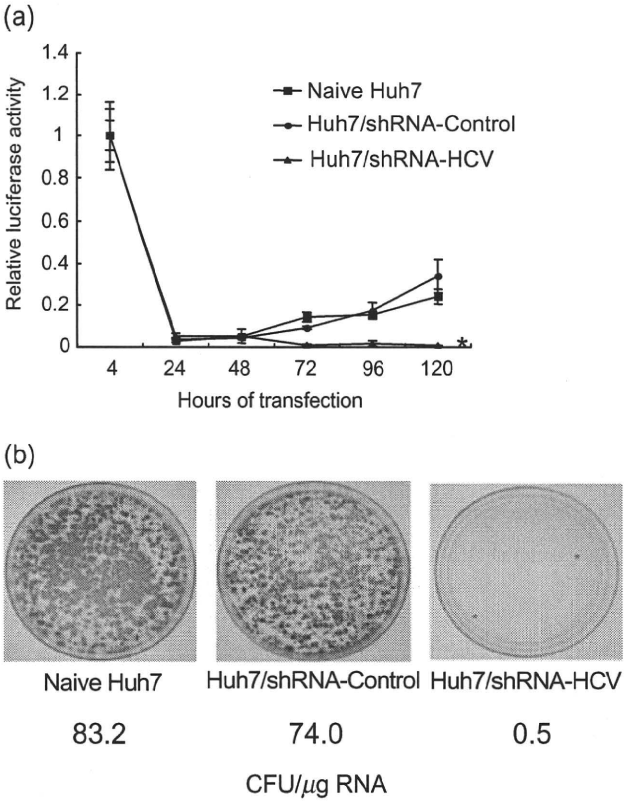

Figure 3 HCV replication can be inhibited by shRNA-HCV which was stably transfected into cells. Huh7/shRNA-HCV and Huh7/shRNA-Control stably express shRNA-HCV or shRNA-Control, respectively, following retroviral transduction. (a) Transient replication assay. An HCV replicon RNA, pRep-Fluc, was transfected into naive Huh7, Huh7/shRNA-HCV and Huh7/shRNA-Control cells. Luciferase activities of the cell lysates were measured serially at the times indicated, and the values were plotted as ratios relative to luciferase activities at 4 h. The luciferase activities at 4 h represent transfected replicon RNA. The data are mean ± SD. An asterisk denotes a *P*-value of less than 0.001 compared with the corresponding value of the naive Huh7 cells. (b) Stable colony formation assay. The HCV replicon, pRep-BSD, was transfected into naive Huh7, Huh7/shRNA-HCV and Huh7/shRNA-Control cells. The cells were cultured in the presence of blasticidin S (BSD) in the medium for ~3 weeks, and the BSD-resistant colonies were counted. These assays were repeated twice. The colony-forming units per microgram RNA (CFU/μg RNA) are shown at the bottom.

Absence of interferon-stimulated gene responses by siRNA delivery

It has been reported that double-stranded RNA may induce interferon-stimulated gene (ISG) responses which cause instability of mRNA, translational suppression of proteins and apoptotic cell

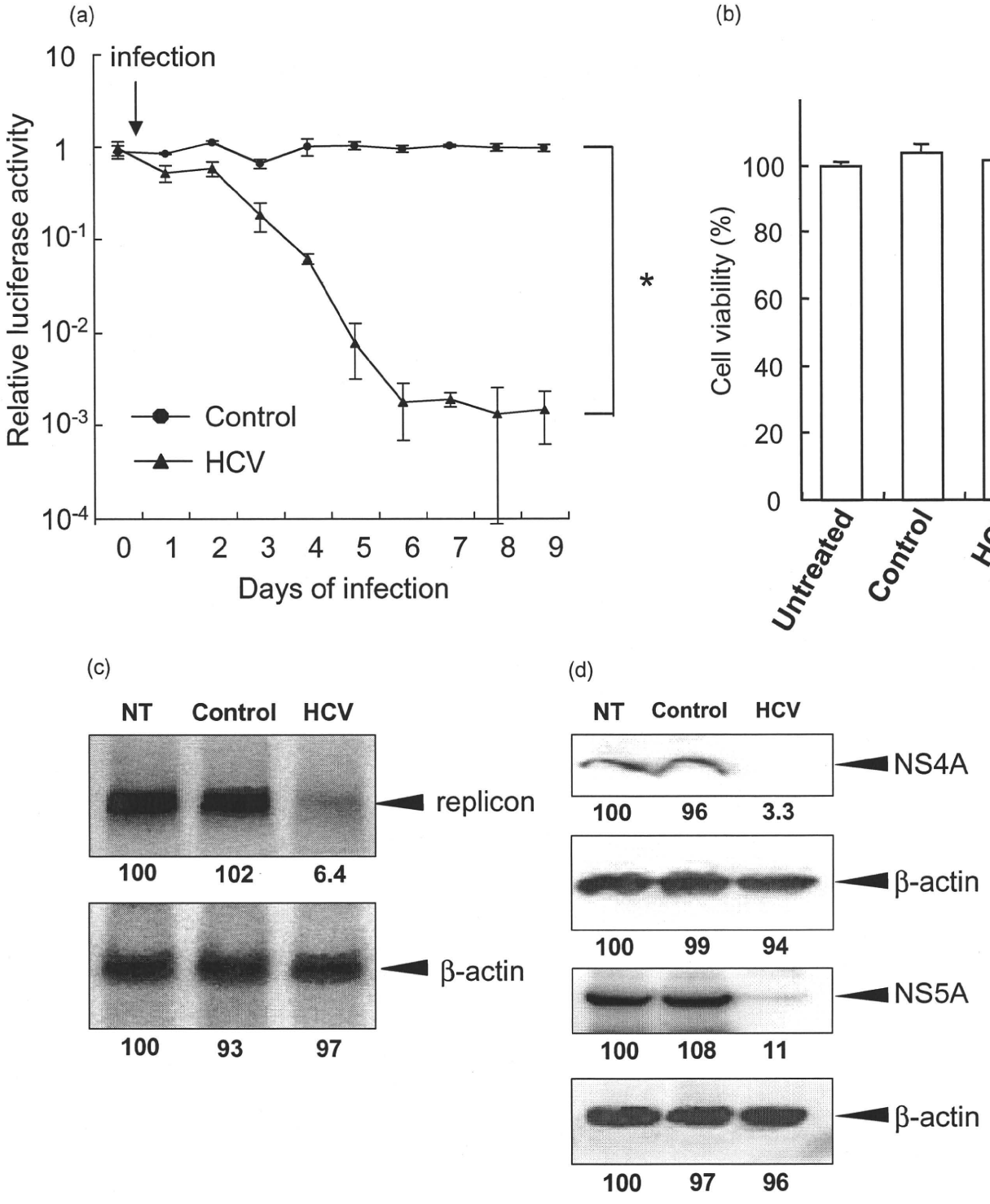

death.[18,30,31] Therefore, we examined the effects of the shRNA-expressing plasmids and adenoviruses on the activation of ISG expression in cells. The ISRE-reporter plasmid, pISRE-TA-Luc, and a control plasmid, peGFPneo, were transfected into Huh7 cells with plasmid pUC19-shRNA-HCV or pUC19-shRNA-Control, or adenovirus, AxshRNA-HCV or AxshRNA-Control, and the ISRE-mediated luciferase activities were measured. On day 2, the ISRE-luciferase activities did not significantly change in cells in which

Figure 4 Effect of a recombinant adenovirus expressing shRNA on HCV replicon. (a) Huh7/pRep-Feo cells were infected with AxshRNA-HCV or shRNA-Control at a multiplicity of infection (MOI) of 1. The cells were harvested, and internal luciferase activities were measured on day 0 though day 9 after adenovirus infection. Each assay was done in triplicate, and the value is displayed as a percentage of no treatment and as mean ± SD. An asterisk indicates a *P*-value of less than 0.05. (b) Dimethylthiazol carboxymethoxyphenyl sulfophenyl tetrazolium (MTS) assay of Huh7/pRep-Feo cells. Cells were infected with indicated recombinant adenoviruses at an MOI of 1. The assay was done at day 6 of infection. Error bars indicate mean + SD. (c) Northern blotting. The upper panel shows replicon RNA, and the lower panel shows beta-actin mRNA. (d) Western blotting. Total cell lysates were separated on NuPAGE gel, blotted and incubated with monoclonal anti-NS4A or anti-NS5A antibodies. The membrane was re-blotted with antibeta-actin antibodies. NT, untreated Huh7/pRep-Feo cells; Control, cells infected with AxshRNA-Control; HCV, cells treated with AxshRNA-HCV. In panels (b) and (c), cells were harvested on day 6 after adenovirus infection at an MOI of 1.

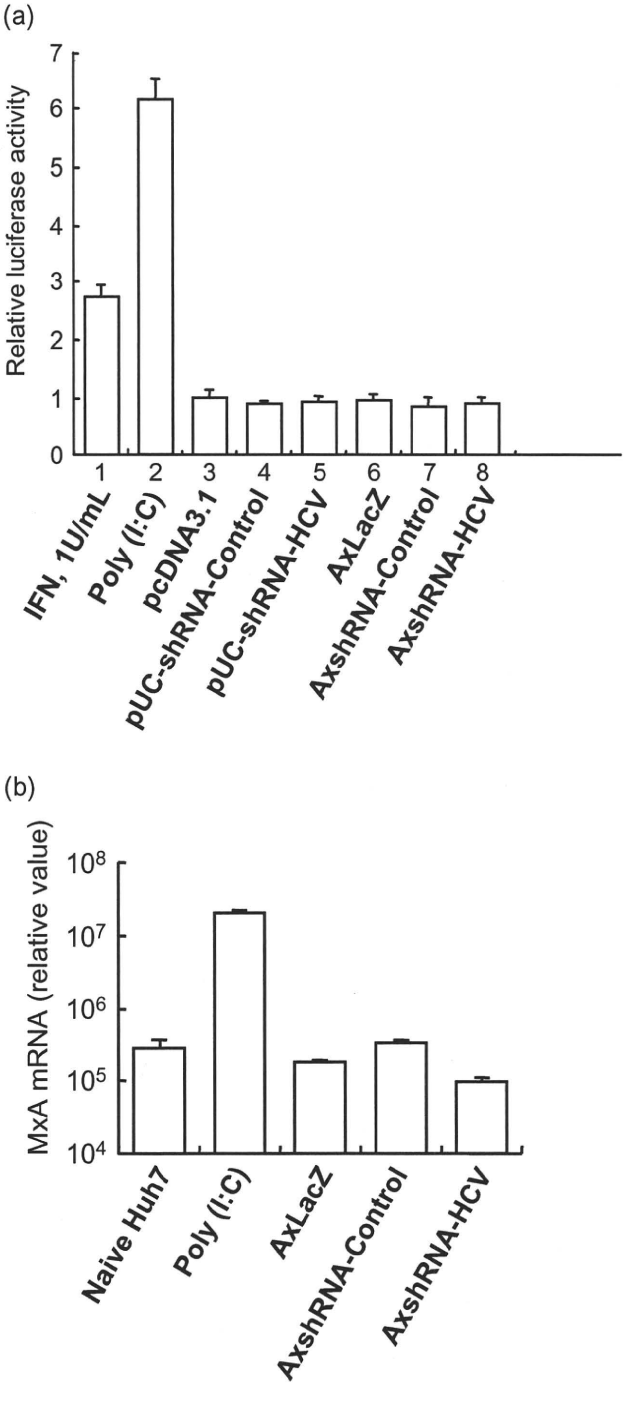

Figure 5 Interferon-stimulated gene responses by transfection of siRNA vectors. (a) Huh7 cells were seeded at 5×10^4 per well in 24-well plates on the day before transfection. As a positive control, 200 ng of pISRE-TA-Luc, or pTA-Luc, 1 ng of pRL-CMV, were transfected into a well using FuGENE-6 Transfection Reagent (Roche), and the cells were cultured with 1 U/mL of interferon (IFN) in the medium (lane 1). Lanes 3–5: 200 ng of pISRE-TA-Luc or pTA-Luc, and 1 ng of pRL-CMV were cotransfected with (lane2) 300 ng of poly (I : C), or 200 ng of plasmids (lane 3) pcDNA3.1, (lane 4) pUC19-shRNA-Control or (lane 5) pUC19-shRNA-HCV. Lanes 6–8: 200 ng of pISRE-TA-Luc or pTA-Luc, and 1 ng of pRL-CMV were transfected, and MOI = 1 of adenoviruses, (lane 6) AxLacZ, which expressed the beta-galactosidase (LacZ) gene under control of the chicken beta-actin (CAG) promoter as a control, (lane 7) AxshRNA-Control or (lane 8) AxshRNA-HCV were infected. Dual luciferase assays were performed at 48 h after transfection. The Fluc activity of each sample was normalized by the respective Rluc activity, and the respective pTA luciferase activity was subtracted from the pISRE luciferase activity. The experiment was done in triplicate, and the data are displayed as means + SD. (b) Huh7 cells were infected with indicated recombinant adenoviruses, AxLacZ, AxshRNA-Control and AxshRNA-HCV. RNA was extracted from each sample at day 6, and mRNA expression levels of an interferon-inducible MxA protein were quantified by the real-time RT-PCR analysis. Primers used were as follows: human MxA sense, 5′-CGA GGG AGA CAG GAC CAT CG-3′; human MxA antisense, 5′-TCT ATC AGG AAG AAC ATT TT-3′; human beta-actin sense, 5′-ACA ATG AAG ATC AAG ATC ATT GCT CCT CCT-3′; and human beta-actin antisense, 5′-TTT GCG GTG GAC GAT GGA GGG GCC GGA CTC-3′.

negative- or positive-control shRNA plasmids was transfected. (Fig. 5a). Similarly, the expression levels of an interferon-inducible MxA protein did not significantly change by transfection of shRNA-expression vectors (Fig. 5b). These results demonstrate that the shRNA used in the present study lack induction of the ISG responses both in the form of the expression plasmids and the adenovirus vectors.

Effect of siRNA and shRNA adenoviruses on HCV-JFH1 cell culture

The effects of HCV-targeted siRNA- and shRNA-expressing adenoviruses were confirmed by using HCV-JFH1 virus cell culture system. Transfection of the siRNA #331[14] into HCV-infected Huh7.5.1 cells resulted in substantial decrease of intracellular HCV RNA, while a control siRNA showed no effect (Fig. 6a). Similarly, infection of AxshRNA-HCV into Huh7.5.1/HCV-JFH1 cells specifically suppressed expression of HCV RNA (Fig. 6b).

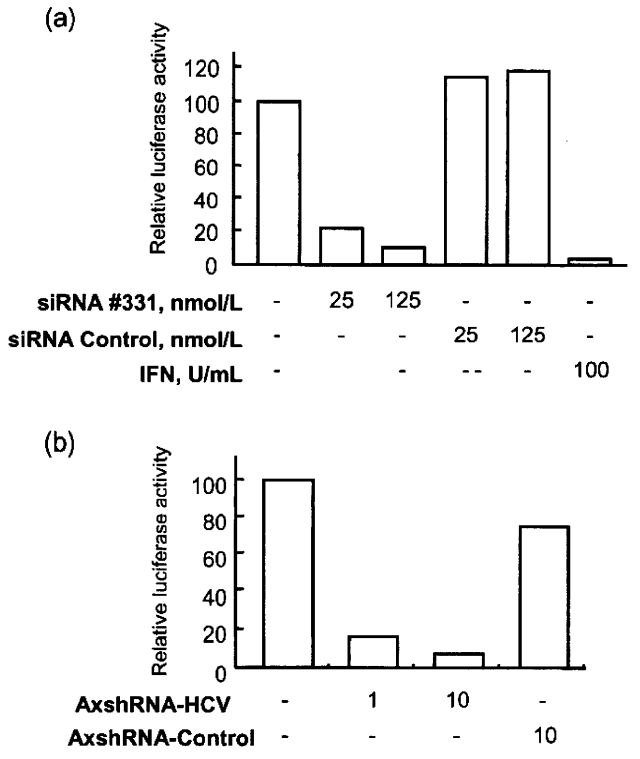

Figure 6 Effects of an siRNA and adenovirus expressing shRNA on HCV-JFH1 cell culture. (a) The siRNA #331, the siRNA-Control[14], (b) AxshRNA-HCV or AxshRNA-Control were, respectively, transfected or infected onto HV-JFH1-infected Huh7.5.1 cells. Seventy-two hours of the transfection or infection, expression level of HCV-RNA was quantified by real-time RT-PCR. The assays were repeated twice, and consistent results were obtained. IFN, recombinant interferon-alpha 2b.

Suppression of HCV-IRES-mediated translation *in vivo* by adenovirus expressing shRNA

The effects of the shRNA expression on the expression of the viral structural proteins *in vivo* were investigated using conditional HCV cDNA-transgenic mice, CN2-29.[28] Adenoviruses, AxshRNA-HCV, AxshRNA-Control or AxCAwl were injected into CN2-29 mice in combination with AxCANCre, an adenovirus expressing *Cre* DNA recombinase. The mice were killed on the fourth day after the injection, and the hepatic expression of the HCV core protein was measured. The expressed amounts of the core protein were 143.0 ± 56.2 pg/mg and 108.5 ± 42.4 pg/mg in AxCAwl and AxshRNA-Control-infected mice, respectively, and the expressed amount was significantly lower in mice injected with AxshRNA-HCV (28.7 ± 7.0 pg/mg, $P < 0.05$, Fig. 7a). Similarly, the induced expression of HCV core protein was not detectable by immunohistochemistry in AxshRNA-HCV infected liver tissue (Fig. 7c). Staining of a host cellular protein, albumin, was not obviously different between the liver infected with AxCAwl, AxshRNA-HCV and AxshRNA-Control (Fig. 7d). The expression levels of two ISG, IFN-beta and Mx1, in the liver tissue were not significantly different between individuals with and without injection of the adenovirus vectors (Fig. 7b). These results indicate specific shRNA silencing of HCV structural protein expression in the liver.

Discussion

The requirements to achieve a high efficiency using RNAi are: (i) selection of target sequences that are the most susceptible to RNAi; (ii) persistence of siRNA activity; and (iii) efficient *in vivo* delivery of siRNA to cells. We have used an shRNA sequence that was derived from a highly efficient siRNA (siRNA331), and constructed a DNA-based shRNA expression cassette that showed competitive effects with the synthetic siRNA (Fig. 2).[14] The shRNA-expression cassette does not only allow extended half-life of the RNAi, but also enables use of gene-delivery vectors, such as virus vectors. As shown in the results, a retrovirus vector expressing shRNA-HCV could stably transduce cells to express HCV-directed shRNA, and the cells acquired protection against HCV subgenomic replication (Fig. 3). An adenovirus vector expressing shRNA-HCV resulted in suppression of HCV subgenomic and protein expression by around three logs to almost background levels (Fig. 4). Consistent results were obtained by using an HCV cell culture (Fig. 6). More importantly, we have demonstrated *in-vivo* effects on viral protein expression in the liver using a conditional transgenic mouse model (Fig. 7). These results suggest that efficient delivery of siRNA could be effective against HCV infection *in vivo*.

An obstacle to applying siRNA technology to treat virus infections is that viruses are prone to mutate during their replication.[32] HCV continuously produces mutated viral strains to escape immune defense mechanisms. Even in a single patient, the circulating HCV population comprises a large number of closely related HCV sequence variants called quasispecies. Therefore, siRNA targeting the protein-coding sequence of the HCV genome, which have been reported by others,[15–19] may vary considerably among different HCV genotypes, and even among strains of the same genotype.[33] Our shRNA sequence targeted the 5′-UTR of HCV RNA, which is the most conserved region among various HCV isolates.[33] In addition, the structural constraints on the 5′-UTR, in terms of its requirement to direct internal ribosome entry and translation of viral proteins, might not permit the evolution of escape mutations. Our preliminary results have shown that the siRNA-HCV suppressed replication of an HCV genotype 2a replicon[34] to the same extent as the HCV 1b replicon.

Although the siRNA techniques rely on a high degree of specificity, several studies report siRNA-induced non-specific effect that may result from induction of ISG responses.[18,31] These effects may be mediated by activation of double-strand RNA-dependent protein kinase, toll-like receptor 3,[35] or possibly by a recently identified RNA helicase, RIG-I.[36] It remains to be determined whether these effects are generally induced by every siRNA construct. Sledz *et al.* have reported that transfection of two siRNA induced cellular interferon responses,[37] while Bridge *et al.* report that shRNA-expressing plasmids induced an interferon response but transfection of synthetic siRNA did not.[31] Speculatively, these effects on the interferon system might be construct dependent. Our shRNA-expression plasmids and adenoviruses did not activate ISG responses *in vitro* (Fig. 5a,b) or *in vivo* (Fig. 7b). We have preliminarily detected phosphorylated PKR (P-PKR) by western

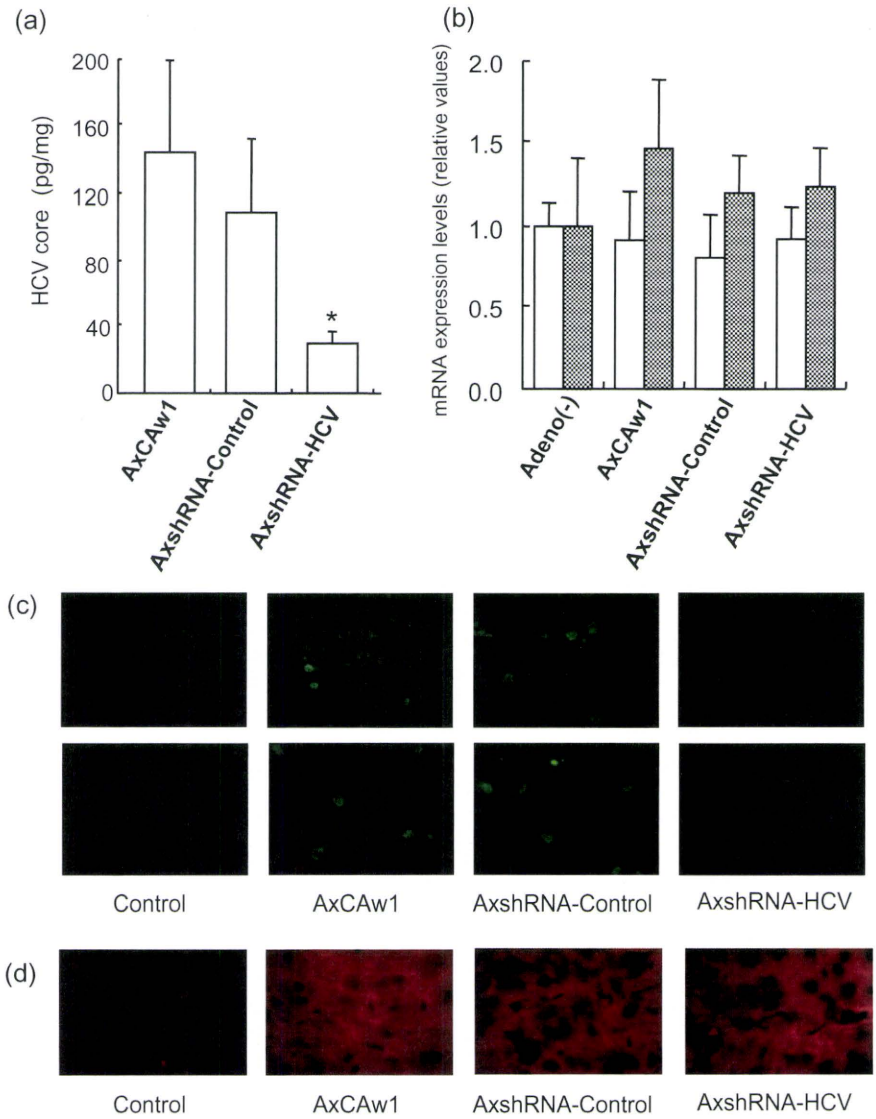

Figure 7 Effects of a recombinant adenovirus expressing shRNA on HCV core protein expression in CN2-29 transgenic mice. CN2-29 transgenic mice were administered with 1×10^9 PFU of AxCANCre combined with 6.7×10^8 PFU of AxshRNA-HCV, AxshRNA or AxCAw1. The mice were killed on day 4 after injection. (a) Quantification of HCV core protein in liver. Liver tissues were homogenized and used to determine the amount of HCV core protein. Each assay was done in triplicate, and the values are displayed as mean ± SD. Asterisk indicates *P*-value of less than 0.05. (b) Expression levels of mouse interferon-beta (white bars) and Mx1 (shaded bars) mRNA in the mouse liver tissue were quantified by the real-time RT-PCR analyses. Primers used were as follows: mouse interferon-beta sense, 5′-ACA GCC CTC TCC ATC AAC TA-3′; mouse interferon-beta antisense, 5′-CCC TCC AGT AAT AGC TCT TC-3′; mouse Mx1 sense, 5′-AGG AGT GGA GAG GCA AAG TC-3′; mouse Mx1 antisense, 5′-CAC ATT GCT GGG GAC TAC CA-3′; mouse beta-actin sense, 5′-ACT CCT ATG TGG GTG ACG AG-3′; mouse beta-actin antisense, 5′-ATA GCC CTC GTA GAT GGG CA-3′. Adeno (-) denotes mice without adenovirus administration. (c) Immunofluorescence microscopy of HCV core protein in the liver tissue. Liver sections of mice were stained using rabbit anticore polyclonal antibody and normal rabbit IgG as a negative control. The upper photographs were obtained at 400× magnification, and the lower photographs were at 1000×. (d) Immunofluorescence microscopy of albumin in liver. Liver sections from the mice were fixed and stained using rabbit antialbumin antibody and normal rabbit IgG as a negative control.

blotting, and found no apparent increase of P-PKR (data not shown). These results indicate that these target sequences and structures are of sufficient specificity to silence the target gene without eliciting non-specific interferon responses.

Beside the canonical action of siRNA, a sequence-specific cleavage of target mRNA, the siRNA could act as a micro-RNA that suppresses translational initiation of mRNA,[38] or it could mediate transcriptional gene silencing.[39] Regarding our *in-vivo* experiments, it was difficult to differentially analyze the effect of siRNA at individual sites of action because post-translational effect of siRNA concomitantly destabilizes target mRNA, which leads to apparent decrease of mRNA transcripts.

Efficiency and safety of gene transfer methods are the key determinants of the clinical success of gene therapy and an unresolved problem. There are several reports of delivery of siRNA or siRNA-expression vectors to cells *in vivo*;[12,40,41] however, gene delivery methods that are safe enough to apply to clinical therapeutics are currently under development. Adenovirus vectors are one of the most commonly used carriers for human gene therapies.[42–44] Our present results demonstrate that the adenoviral delivery of shRNA is effective in blocking HCV replication *in vitro* and virus protein expression *in vivo*. Adenovirus vectors have several advantages of efficient delivery of transgene both *in vitro* and *in vivo* and natural hepatotropism when administered *in vivo*. The AxshRNA-HCV specifically blocked expression of HCV structural proteins in a conditional transgenic mouse expressing those proteins. The current adenovirus vectors may cause inflammatory reactions in the target organ,[45] however, and produce neutralizing antibodies which make repeated administration difficult. These problems may be overcome by the improved constructs of virus vectors with attenuated immunogenicity or by the development of non-viral carriers for gene delivery.[46]

In conclusion, our results demonstrate the effectiveness and feasibility of the siRNA expression system. The efficiency of adenovirus expressing shRNA that target HCV suggests that delivery and expression of siRNA in hepatocytes may eliminate the virus and that this RNA-targeting approach might provide a potentially effective future therapeutic option for HCV infection.

Acknowledgments

This study was supported by grants from Japan Society for the Promotion of Science, 15590629 and 16590580, and partly supported by a grant from the Viral Hepatitis Research Foundation of Japan.

References

1 Alter MJ. Epidemiology of hepatitis C. *Hepatology* 1997; **26**: 62S–65S.
2 Hadziyannis SJ, Sette H Jr, Morgan TR *et al.* Peginterferon-alpha2a and ribavirin combination therapy in chronic hepatitis C: a randomized study of treatment duration and ribavirin dose. *Ann. Intern. Med.* 2004; **140**: 346–55.
3 Fire A, Xu S, Montgomery M, Kostas S, Driver S, Mello C. Potent and specific genetic interference by double-stranded RNA in Caenorhabditis elegans. *Nature* 1998; **19**: 806–11.
4 Elbashir SM, Harborth J, Lendeckel W, Yalcin A, Weber K, Tuschl T. Duplexes of 21-nucleotide RNAs mediate RNA interference in cultured mammalian cells. *Nature* 2001; **411**: 494–8.
5 Coburn GA, Cullen BR. Potent and specific inhibition of human immunodeficiency virus type 1 replication by RNA interference. *J. Virol.* 2002; **76**: 9225–31.
6 Jacque JM, Triques K, Stevenson M. Modulation of HIV-1 replication by RNA interference. *Nature* 2002; **418**: 435–8.
7 Gitlin L, Karelsky S, Andino R. Short interfering RNA confers intracellular antiviral immunity in human cells. *Nature* 2002; **418**: 430–4.
8 Ge Q, Filip L, Bai A, Nguyen T, Eisen HN, Chen J. Inhibition of influenza virus production in virus-infected mice by RNA interference. *Proc. Natl. Acad. Sci. USA* 2004; **101**: 8676–81.
9 Wang C, Pflugheber J, Sumpter R Jr *et al.* Alpha interferon induces distinct translational control programs to suppress hepatitis C virus RNA replication. *J. Virol.* 2003; **77**: 3898–912.
10 Klein C, Bock CT, Wedemeyer H *et al.* Inhibition of hepatitis B virus replication in vivo by nucleoside analogues and siRNA. *Gastroenterology* 2003; **125**: 9–18.
11 Konishi M, Wu CH, Wu GY. Inhibition of HBV replication by siRNA in a stable HBV-producing cell line. *Hepatology* 2003; **38**: 842–50.
12 McCaffrey AP, Meuse L, Pham TT, Conklin DS, Hannon GJ, Kay MA. RNA interference in adult mice. *Nature* 2002; **418**: 38–9.
13 Shlomai A, Shaul Y. Inhibition of hepatitis B virus expression and replication by RNA interference. *Hepatology* 2003; **37**: 764–70.
14 Yokota T, Sakamoto N, Enomoto N *et al.* Inhibition of intracellular hepatitis C virus replication by synthetic and vector-derived small interfering RNAs. *EMBO Rep.* 2003; **4**: 602–8.
15 Kapadia SB, Brideau-Andersen A, Chisari FV. Interference of hepatitis C virus RNA replication by short interfering RNAs. *Proc. Natl. Acad. Sci. USA* 2003; **100**: 2014–18.
16 Kronke J, Kittler R, Buchholz F *et al.* Alternative approaches for efficient inhibition of hepatitis C virus RNA replication by small interfering RNAs. *J. Virol.* 2004; **78**: 3436–46.
17 Randall G, Grakoui A, Rice CM. Clearance of replicating hepatitis C virus replicon RNAs in cell culture by small interfering RNAs. *Proc. Natl. Acad. Sci. USA* 2003; **100**: 235–40.
18 Seo MY, Abrignani S, Houghton M, Han JH. Letter to the editor: small interfering RNA-mediated inhibition of hepatitis C virus replication in the human hepatoma cell line Huh-7. *J. Virol.* 2003; **77**: 810–12.
19 Wilson JA, Jayasena S, Khvorova A *et al.* RNA interference blocks gene expression and RNA synthesis from hepatitis C replicons propagated in human liver cells. *Proc. Natl. Acad. Sci. USA* 2003; **100**: 2783–8.
20 Guo JT, Bichko VV, Seeger C. Effect of alpha interferon on the hepatitis C virus replicon. *J. Virol.* 2001; **75**: 8516–23.
21 Tanabe Y, Sakamoto N, Enomoto N *et al.* Synergistic inhibition of intracellular hepatitis C virus replication by combination of ribavirin and interferon-alpha. *J. Infect. Dis.* 2004; **189**: 1129–39.
22 Maekawa S, Enomoto N, Sakamoto N *et al.* Introduction of NS5A mutations enables subgenomic HCV-replicon derived from chimpanzee-infectious HC-J4 isolate to replicate efficiently in Huh-7 cells. *J. Viral. Hepat.* 2004; **11**: 394–403.
23 Miyagishi M, Sumimoto H, Miyoshi H, Kawakami Y, Taira K. Optimization of an siRNA-expression system with an improved hairpin and its significant suppressive effects in mammalian cells. *J. Gene Med.* 2004; **6**: 715–23.
24 Li Y, Yokota T, Matsumura R, Taira K, Mizusawa H. Sequence-dependent and independent inhibition specific for mutant ataxin-3 by small interfering RNA. *Ann. Neurol.* 2004; **56**: 124–9.
25 Kanazawa N, Kurosaki M, Sakamoto N *et al.* Regulation of hepatitis C virus replication by interferon regulatory factor-1. *J. Virol.* 2004; **78**: 9713–20.
26 Wakita T, Pietschmann T, Kato T *et al.* Production of infectious hepatitis C virus in tissue culture from a cloned viral genome. *Nat. Med.* 2005; **11**: 791–6.
27 Zhong J, Gastaminza P, Cheng G *et al.* Robust hepatitis C virus infection in vitro. *Proc. Natl. Acad. Sci. USA* 2005; **102**: 9294–9.
28 Wakita T, Taya C, Katsume A *et al.* Efficient conditional transgene expression in hepatitis C virus cDNA transgenic mice mediated by the Cre/loxP system. *J. Biol. Chem.* 1998; **273**: 9001–6.
29 Kashiwakuma T, Hasegawa A, Kajita T *et al.* Detection of hepatitis C virus specific core protein in serum of patients by a sensitive fluorescence enzyme immunoassay (FEIA). *J. Immunol. Methods* 1996; **28**: 79–89.

30 Baglioni C, Nilsen TW. Mechanisms of antiviral action of interferon. *Interferon* 1983; **5**: 23–42.
31 Bridge A, Pebernard S, Ducraux A, Nicoulaz A, Iggo R. Induction of an interferon response by RNAi vectors in mammalian cells. *Nat. Genet.* 2003; **34**: 263–4.
32 Carmichael GG. Silencing viruses with RNA. *Nature* 2002; **418**: 379–80.
33 Okamoto H, Okada S, Sugiyama Y *et al.* Nucleotide sequence of the genomic RNA of hepatitis C virus isolated from a human carrier: comparison with reported isolates for conserved and divergent regions. *J. Gen. Virol.* 1991; **72**: 2697–704.
34 Kato T, Date T, Miyamoto M *et al.* Efficient replication of the genotype 2a hepatitis C virus subgenomic replicon. *Gastroenterology* 2003; **125**: 1808–17.
35 Alexopoulou L, Holt AC, Medzhitov R, Flavell RA. Recognition of double-stranded RNA and activation of NF-kB by Toll-like receptor 3. *Nature* 2001; **413**: 732–8.
36 Yoneyama M, Kikuchi M, Natsukawa T *et al.* The RNA helicase RIG-I has an essential function in double-stranded RNA-induced innate antiviral responses. *Nat. Immunol.* 2004; **5**: 730–7.
37 Sledz C, Holko M, de Veer M, Silverman R, Williams, B. Activation of the interferon system by short-interfering RNAs. *Nat. Cell. Biol.* 2003; **5**: 834–9.
38 Doench JG, Petersen CP, Sharp PA. siRNAs can function as miRNAs. *Genes Dev.* 2003; **17**: 438–42.
39 Morris KV. siRNA-mediated transcriptional gene silencing: the potential mechanism and a possible role in the histone code. *Cell. Mol. Life Sci.* 2005; **62**: 3057–66.
40 Xia H, Mao Q, Paulson HL, Davidson BL. siRNA-mediated gene silencing in vitro and in vivo. *Nat. Biotechnol.* 2002; **20**: 1006–10.
41 Zender L, Hutker S, Liedtke C *et al.* Caspase 8 small interfering RNA prevents acute liver failure in mice. *Proc. Natl. Acad. Sci. USA* 2003; **100**: 7797–802.
42 Akli S, Caillaud C, Vigne E *et al.* Transfer of a foreign gene into the brain using adenovirus vectors. *Nat. Genet.* 1993; **3**: 224–8.
43 Bajocchi G, Feldman SH, Crystal RG, Mastrangeli A. Direct in vivo gene transfer to ependymal cells in the central nervous system using recombinant adenovirus vectors. *Nat. Genet.* 1993; **3**: 229–34.
44 Davidson BL, Allen ED, Kozarsky KF, Wilson JM, Roessler BJ. A model system for in vivo gene transfer into the central nervous system using an adenoviral vector. *Nat. Genet.* 1993; **3**: 219–23.
45 Yang Y, Wilson JM. Clearance of adenovirus-infected hepatocytes by MHC class I-restricted CD4+ CTLs in vivo. *J. Immunol.* 1995; **155**: 2564–70.
46 Fleury S, Driscoll R, Simeoni E *et al.* Helper-dependent adenovirus vectors devoid of all viral genes cause less myocardial inflammation compared with first-generation adenovirus vectors. *Basic Res. Cardiol.* 2004; **99**: 247–56.

Cell Death and Differentiation (2008) 15, 1691–1700

www.nature.com/cdd

Focal degeneration of astrocytes in amyotrophic lateral sclerosis

D Rossi*[,1], L Brambilla[1,4], CF Valori[1,4,5], C Roncoroni[1], A Crugnola[1], T Yokota[2], DE Bredesen[2] and A Volterra[1,3]

Astrocytes emerge as key players in motor neuron degeneration in Amyotrophic Lateral Sclerosis (ALS). Whether astrocytes cause direct damage by releasing toxic factors or contribute indirectly through the loss of physiological functions is unclear. Here we identify in the hSOD1^{G93A} transgenic mouse model of ALS a degenerative process of the astrocytes, restricted to those directly surrounding spinal motor neurons. This phenomenon manifests with an early onset and becomes significant concomitant with the loss of motor cells and the appearance of clinical symptoms. Contrary to wild-type astrocytes, mutant hSOD1-expressing astrocytes are highly vulnerable to glutamate and undergo cell death mediated by the metabotropic type-5 receptor (mGluR5). Blocking mGluR5 *in vivo* slows down astrocytic degeneration, delays the onset of the disease and slightly extends survival in hSOD1^{G93A} transgenic mice. We propose that excitotoxicity in ALS affects both motor neurons and astrocytes, favouring their local interactive degeneration. This new mechanistic hypothesis has implications for therapeutic interventions.
Cell Death and Differentiation (2008) **15,** 1691–1700; doi:10.1038/cdd.2008.99; published online 11 July 2008

Amyotrophic Lateral Sclerosis (ALS) is a neurodegenerative disorder characterized by the progressive degeneration of corticospinal and spinal motor neurons. In about 1–2% of patients, the disease is linked to mutations in the gene coding for Cu-Zn superoxide dismutase (SOD1).[1] Transgenic animals[2–4] that overexpress mutant human SOD1s (hSOD1s) develop progressive ALS-like disease. The cascade of events ultimately responsible for motor neuron degeneration, however, remains elusive.

Important insights come from the observations that death of motor cells involves both cell-autonomous and non-cell-autonomous disease mechanisms, implying that mutant hSOD1 expression in neurons is sufficient to trigger the disease,[5] but also the interaction of motor neurons with the neighboring glial cells contributes to the deleterious process.[6] These observations have brought attention to the abnormalities affecting glial cells in ALS. In both human cases and animal models, microglia and astrocytes undergo massive activation in regions of motor neuron loss.[7,8] Microglial alterations were shown to be implicated in disease progression in transgenic mice[7,9] and the contribution of astrocytes to motor neuron degeneration is gaining more and more consideration. A recent study reports that mutant hSOD1 expression in astrocytes leads to motor neuron damage and accelerated disease progression by controlling microglial activation.[8] Moreover, astrocytes expressing mutant hSOD1 were reported to release factors selectively toxic for motor neurons *in vitro*.[10,11] The presence of mutant hSOD1 in these cells was also described to perturb protective functions of astrocytes towards neurons. While normal astrocytes regulate the expression of the GluR2 subunit of the AMPA receptors in motor neurons, the expression of mutant hSOD1 abolishes this property.[12] Furthermore, both ALS patients and transgenic animals exhibit a defect of the astrocyte-selective glutamate transporter EAAT2/GLT1.[3,4,13] EAAT2/GLT1 is crucial for controlling the physiological clearance of extracellular glutamate in the spinal cord. Thus, its loss may lead to excitotoxic glutamate levels and this could contribute to the disease progression.[14–16] Another peculiar abnormality of astrocytes in hSOD1 mutant mice is the presence of Lewy body-like inclusions containing SOD1 and ubiquitin.[3] Interestingly, such inclusions are the earliest indicator of disease in

[1]Department of Pharmacological Sciences, Center of Excellence on Neurodegenerative Diseases, University of Milan, Via Balzaretti 9, Milan 20133, Italy; [2]Buck Institute for Age Research, 8001 Redwood Blvd, Novato, CA 94945, USA and [3]Department of Cell Biology and Morphology, University of Lausanne, Rue du Bugnon 9, Lausanne 1005, Switzerland

*Corresponding author: D Rossi, Department of Pharmacological Sciences, Center of Excellence on Neurodegenerative Diseases, , University of Milan, Via Balzaretti 9, 20133 Milan, Italy. Tel: +39 02 5031 8327; Fax: +39 02 5031 8284; E-mail: daniela.rossi@unimi.it

[4]These authors contributed equally to this work

[5]Current address: Academic Neurology Unit, University of Sheffield, Beech Hill Road, Sheffield S10 2RX, UK

Keywords: amyotrophic lateral sclerosis; apoptosis; astrocyte; excitotoxicity; metabotropic glutamate receptor

Abbreviations: ALS, amyotrophic lateral sclerosis; hSODI, human superoxide dismutase 1; AMPA, alpha-amino-3-hydxoxy-5-methyl-4-isoxazolepropionic acid; GluR2, AMPA receptor GluR2 subunit; EAAT2/GLT1, excitatory amino acid transporter 2/glutamate transporter 1; GFAP, glial fibrillary acidic protein; SGPCs, spheroid GFAP-positive cells; SMI32, anti-nonphosphorylated neurofilament H antibody from Sternberger Monoclonals Incorporated; SOD1^{G85R}, SOD1 harboring a single amino acid substitution of glycine to arginine at codon 85; SODI^{G93A}, SOD1 harboring a single amino acid substitution of glycine to alanine at codon 93; SOD1^{WT}, wild-type SOD1; VGLUT1, vesicular glutamate transporter 1; EAAT1/GLAST, excitatory amino acid transporter 1/glutamate aspartate transporter; TBOA, DL-threo-β-benzyloxyaspartate; mGluR, metabotropic glutamate receptor; MCPG, (S)-α-methyl-4-carboxyphenylglycine; CNQX, 6-cyano-7-nitroquinoxaline-2,3-dione; GYK1 52466, 4-(8-Methyl-9H-1,3-dioxolo[4,5-h][2,3]benzodiazepin-5-yl)-benzenamine; MPEP, 2-methyl-6-(phenylethynyl)-pyridine; mGluR5, metabotropic subtype 5 glutamate receptor; DHPG, (RS)-3,5-dihydroxyphenylglycine; DLTD, Asp-Leu-Thr-Asp; NG2, chondroitin sulfate proteoglycan; GDH, glutamate dehydrogenase

Received 26.10.07; revised 19.5.08; accepted 20.5.08; Edited by L Green; published online 11.7.08

hSOD1^{G85R} mice, a transgenic line developing a late-onset, ultrarapid disease progression. Similar inclusions containing activated caspase-3 were subsequently reported in the same hSOD1^{G85R} mice, as well as in hSOD1^{G93A} mice,[17] a transgenic line showing earlier onset but analogously fast disease progression. However, the significance of such astrocytic inclusions remains elusive.

Here, we report in the spinal cord of hSOD1^{G93A} mice that a subset of astrocytes harboring protein inclusions undergoes morphological and biochemical changes that are reminiscent of degenerating cells. Moreover, we demonstrate that the expression of mutant hSOD1s makes astrocytes vulnerable to glutamate through the activation of mGluR5 and that blockage of mGluR5 *in vivo* reduces astrocyte degeneration, postpones disease onset and extends lifespan.

Results

Presence of abnormal spheroid-shaped astrocytes in the lumbar spinal cord of hSOD1^{G93A} mice. To study the morphological and structural changes of astrocytes during the progression of the disease, we first performed immunohistochemical analysis of lumbar spinal cord sections from hSOD1^{G93A} and hSOD1^{WT} transgenic mice,[2] using the glial fibrillary acidic protein (GFAP) as an astrocytic marker. While no gross abnormalities were detected in the spinal cord of hSOD1^{WT} mice (Figure 1a), we found that most of the GFAP-positive cells present in sections from end-stage hSOD1^{G93A} animals resembled typical reactive astrocytes with elaborated networks of long processes. In addition, we identified a subpopulation of cells displaying fully distinct features (Figure 1b). These cells exhibited a spheroid-shaped cell body with an increased diameter (mean ± S.E.M.: 13.37 ± 0.35 μm; range: 6.7–34 μm; $n=88$ from six mice) compared to resting astrocytes (9.39 ± 0.13 μm; range: 4.9–15.9 μm; $n=145$ from 6 mice). This unusual morphology was concomitant with a reduction or even absence of GFAP-positive processes, which appeared short and abnormally thick. Immunohistochemical analysis revealed that all of the spheroid GFAP-positive cells (SGPCs) were positive for ubiquitin, which occupied most of the spheroid diameter and overlapped with the compact cap of GFAP (Figure 1c and d). Cells showing thick processes projecting off the cell body exhibited ubiquitin immunoreactivity in both the cell body and the processes (Figure 1c). About one-third of the SGPCs were immunopositive for the active form of caspase-3 (Figure 1e and f). In general, active caspase-3 labeling had a characteristic annular shape and was circumscribed by a GFAP cap (Figure 1e), which appeared thinner and less compact than in the caspase-3-negative SGPCs (Figure 1d and f). Furthermore, active caspase-3-positive SGPCs had less GFAP-positive processes compared to caspase-3-negative SGPCs.

SGPCs appear selectively in the microenvironment of motor neurons before the symptomatic phase of ALS. To investigate whether the presence of SGPCs correlated with the area of the spinal cord affected by the disease, we focused on the distribution of these cells. Importantly, we found that they were placed exclusively in the ventral horns, where motor neurons are located, while reactive astrocytes were present both in the ventral and dorsal horn regions and in the white matter (Figure 2). To more specifically analyze the distribution of SGPCs in relation to motor neurons, we measured the interdistance between SGPCs and the motor neuron cell bodies labeled with SMI32. SGPCs resulted strictly confined to the microenvironment of motor neurons. In fact, 93% of the spheroid astrocytic cells were located within a 130 μm radius of one to seven motor neurons. In 88% of the cases, the interdistance between the SGPC and the closest motor neuron was $\leqslant 40\,\mu$m, and in 31% it was $\leqslant 10\,\mu$m (Figure 1g).

To explore this phenomenon in more detail, we then looked at the time-course of SGPC formation (Figure 3). Ubiquitin-labeled SGPCs appeared around motor neurons for the first time in 75-day-old mice (Figure 3). Their number increased by 21-fold at 100 days and by 57-fold at the end stage (Figure 3e). Analysis of the time-course of caspase-3 levels in SGPCs revealed that the active caspase-3 appeared at 100 days of age and was present in 18% of the spheroid cells. At the end stage, the percentage of active caspase-3-positive SGPCs had grown to 33% (Figure 3e). Parallel analysis of the neighboring motor neurons revealed a decline of motor cell number, which became statistically significant at around 100 days of age and occurred in parallel to the appearance of the first signs of motor impairment (Figure 7a).[14,18] Therefore, SGPC formation precedes motor neuron loss and becomes considerable in parallel to degeneration of motor cells and appearance of clinical signs.

Active caspase-3 cleaves the astrocyte GFAP cytoskeleton. The fact that active caspase-3 appears in SGPCs at late time points, when the disease has already progressed, could reflect an advanced state of degeneration of the cells. In fact, the GFAP labeling of active caspase-3-positive SGPCs appeared weaker and less compact compared to caspase-3-negative SGPCs (Figure 1d and f).

Interestingly, caspase-3 was recently shown to cleave GFAP in degenerating astrocytes in Alzheimer's disease, producing a 20 kDa GFAP carboxy-terminal fragment.[19] To investigate whether caspase-3 activity might be responsible for GFAP cleavage in hSOD1^{G93A} mice, we performed western blot analysis on spinal cord homogenates from end-stage hSOD1^{G93A} mice (Figure 4). Homogenates from hSOD1^{G93A} mice contained a low molecular weight GFAP fragment. This fragment had the same mobility of the GFAP fragment obtained by treating homogenates from wild-type mice with recombinant active caspase-3.

Altogether, these data strongly support the conclusion that SGPCs represent a subpopulation of degenerating astrocytes in hSOD1^{G93A} mice.

Expression of mutant hSOD1 confers glutamate vulnerability to astrocytes. Since excitatory afferents and dendrites of spinal motor neurons make synaptic contacts in the ventral horns,[20] that is the area of SGPC formation, we decided to label glutamatergic terminals by double immunostaining with antibodies against the presynaptic marker synaptophysin and the vesicular glutamate transporter 1 (VGLUT1) (Figure 5a). Given that 92 ± 2.3% of VGLUT1-

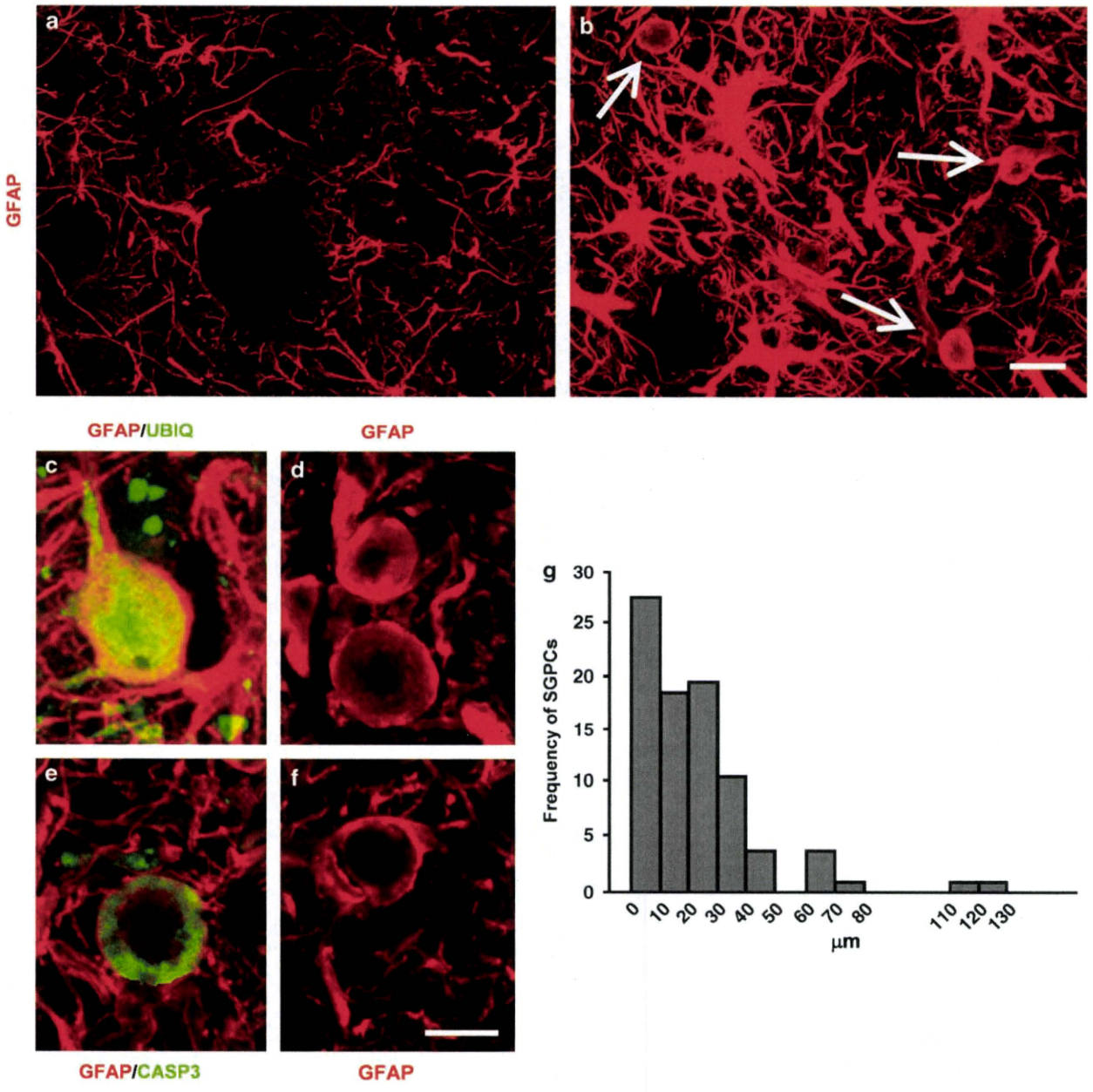

Figure 1 Degenerating astrocytes are located in the motor neuron microenvironment in the ventral lumbar spinal cord of hSOD1^{G93A} mice. (**a** and **b**) Spheroid GFAP-positive cells (SGPCs, arrows) are located together with typical reactive astrocytes in the ventral horns of hSOD1^{G93A} mice at the end stage (**b**), but not in the spinal cord of hSOD1^{WT} transgenic mice (**a**); (**c** and **d**) all SGPCs are immunopositive for ubiquitin: some SGPCs exhibit continuous ubiquitin immunoreactivity in both the cell body and in the processes projecting off the cell body, which appear abnormally thick (**c**); cell bodies present a thick GFAP-positive cap (**d**); (**e** and **f**) SGPCs immunopositive for active caspase-3: notice the eccentric annular appearance of caspase-3 immunoreactivity in the cell body (**e**) and the thin GFAP cap (**f**). Scale bar, 20 μm (**a** and **b**) and 10 μm (**c**–**f**). (**g**) Frequency histogram shows the distribution of spheroid astrocytes around motor neurons in sections from 100-day-old mice ($n = 96$ from six mice). Distance (μm) from the closest motor neuron was measured from the border of the SGPC body to the border of the motor neuron cell body as defined by SMI32 immunostaining. Distances were put into bins of 10 μm and their frequency distribution calculated. Only 7 out of 96 SGPCs had no adjacent motor neurons, though we cannot exclude their presence in contiguous sections

positive puncta colocalized with synaptophysin ($n = 60$ fields from five mice), we concluded that, in the ventral horns of the lumbar spinal cord, VGLUT1 mostly identifies glutamatergic terminals. Using the vesicular transporter as an indicator of excitatory presynapses, we next examined the distribution of VGLUT1-positive boutons in relation to motor neurons and SGPCs. Consistent with previous reports,[20] we confirmed that VGLUT1-immunoreactive terminals surround motor neuron cell bodies and dendrites, as defined by SMI32 staining (Figure 5b). Moreover, they enclose ubiquitin-positive SGPCs around motor cells (Figure 5c and d), suggesting that both cell types could sense glutamate released from those nerve terminals.

Given the altered glutamate handling reported in both sporadic ALS patients and transgenic animals,[3,4,13] we

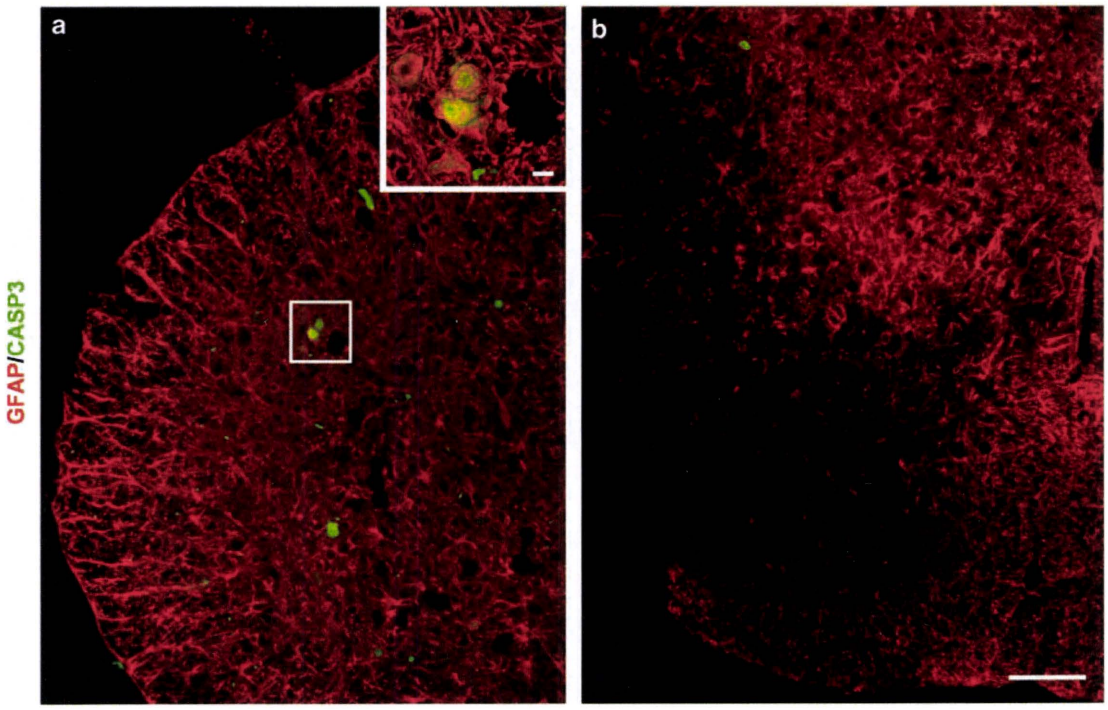

Figure 2 Degenerating astrocytes have confined distribution in the ventral region of the lumbar spinal cord. (**a** and **b**) Double immunofluorescence staining against GFAP and active caspase-3 shows the specific localization of astrocytes containing round inclusions in the ventral horns (square box magnified in inset) (**a**), but not in the dorsal horns of the lumbar spinal cord (**b**). Scale bars, 100 μm (**a** and **b**) and 10 μm (inset)

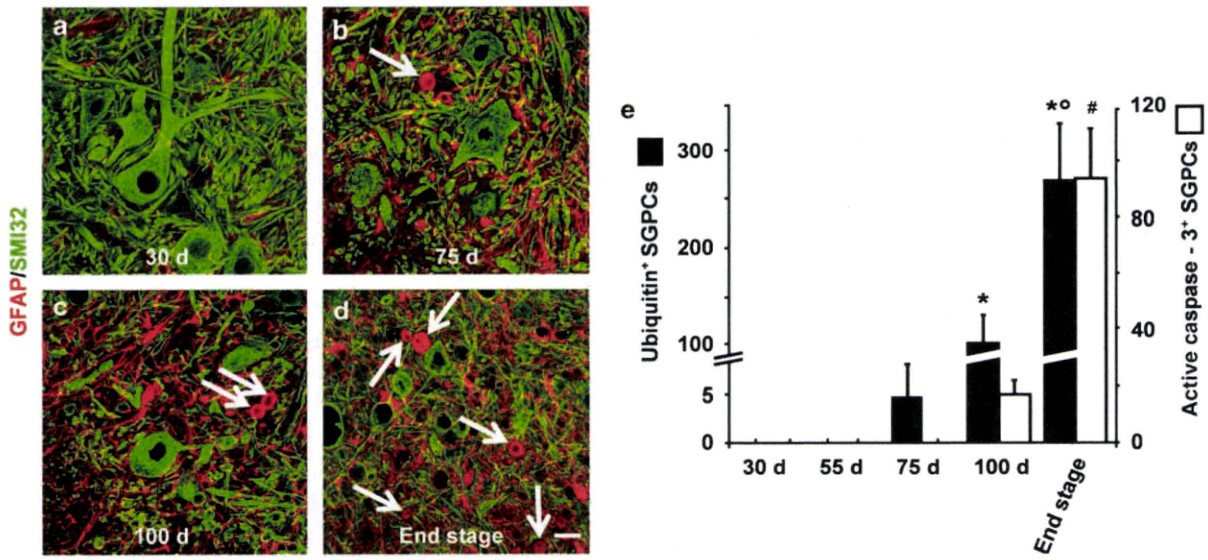

Figure 3 SGPCs appear early during disease progression in hSOD1^{G93A} mice. (**a–d**) An increasing number of SGPCs (arrows) directly contiguous to motor neurons appears during the disease progression. Lumbar spinal cord sections from mice at the age of 30 days (**a**), 75 days (**b**), 100 days (**c**) or at the end stage (**d**) were simultaneously labeled for nonphosphorylated neurofilaments (SMI32 antibody) and GFAP. Scale bar, 20 μm. (**e**) Time course of the appearance of abnormal spheroid astrocytes. Histogram represents the number of SGPCs double fluorescent for GFAP and ubiquitin (black bars) or GFAP and active caspase-3 (white bars, $n = 4$–6 mice for each time point) at different ages during the disease progression. Values are means ± S.E.M. (see Materials and Methods) ($^{*}P < 0.05$ *versus* ubiquitin^{+} SGPCs at 75 days, $^{\circ}P < 0.05$ *versus* ubiquitin^{+} SGPCs at 100 days, $^{\#}P < 0.05$ *versus* caspase-3^{+} SGPCs at 100 days; ANOVA followed by the Fischer PLSD method)

investigated whether SGPCs expressed the glial glutamate transporter EAAT2/GLT1. Immunofluorescence analysis of spinal cord sections from hSOD1^{G93A} mice at the age of 100 days revealed that the SGPCs stain very weakly for this transporter (Supplementary Figure 1). Normally, expression of a highly efficient uptake system makes astrocytes resistant to glutamate concentrations toxic for neurons.[21] To verify if focal astrocytic degeneration might depend on an excitotoxic

mechanism, we prepared astrocytic cultures from the spinal cord of hSOD1^{G93A} mice and exposed them to neurotoxic glutamate concentrations (500 μM, 30 min). We found that a subpopulation of astrocytes underwent delayed caspase-3 activation and nuclear condensation. This phenomenon did not occur in sister cultures of nontransgenic or hSOD1^{WT} astrocytes (Figure 6a, left). In a different type of experiment, we transiently transfected wild-type rat spinal cord astrocytes with wild-type myc-tagged hSOD1 expression vectors (coding for hSOD1^{WT}, hSOD1^{G93A} or hSOD1^{G85R}, respectively).

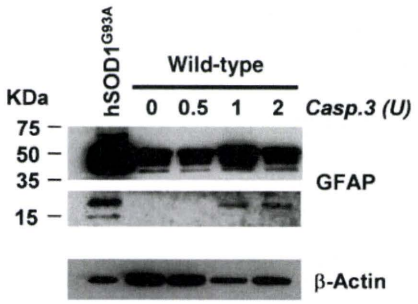

Figure 4 Active caspase-3 cleaves GFAP in the spinal cord from hSOD1^{G93A} mice but not from wild-type mice. Representative immunoblot of spinal cord homogenates from end stage hSOD1^{G93A} mice and age-matched wild-type animals. Wild-type tissues were incubated with an increasing concentration of recombinant active caspase-3 as indicated. The blot was probed with a mouse anti-GFAP monoclonal antibody that recognizes the carboxy-terminal domain of GFAP (clone G-A-5). This revealed both the full-length protein of 50 kDa and the caspase-3-cleaved GFAP fragment of 20 kDa. No labeling of the 20 kDa fragment was obtained in undigested tissue. β-actin was used as loading control

Exposure to glutamate induced delayed caspase-3 activation and nuclear condensation in both hSOD1^{G93A}- and hSOD1^{G85R}-expressing astrocytes, but not in the hSOD1^{WT}-expressing ones (Figure 6a, right). Therefore, expression of mutant hSOD1s confers glutamate vulnerability to astrocytes.

We next estimated the ambient glutamate level ($[Glu]_o$) that is toxic for mutant hSOD1-expressing astrocytes. Since in our experimental conditions cultured astrocytes express both glial glutamate transporters, EAAT1/GLAST and EAAT2/GLT1 (Supplementary Figure 2), we artificially blocked the basal glutamate uptake with the full-spectrum transport inhibitor, DL-*threo*-β-benzyloxyaspartate (TBOA, 200 μM, 30 min). In hSOD1^{G93A} cultures, TBOA raised $[Glu]_o$ to 1.87 ± 0.10 μM ($n = 6$ in triplicate) and triggered the death of subpopulations of astrocytes (Figure 6a, left). In wild-type astrocytes, TBOA enhanced $[Glu]_o$ to the same extent as in hSOD1^{G93A} astrocytes (to 2 ± 0.11 μM), but had no toxic effect. Therefore, ambient glutamate concentrations as low as 2 μM are selectively toxic to astrocytes expressing mutant hSOD1.

The glutamate vulnerability of mutant hSOD1-expressing astrocytes can be ascribed to mGluR5 activation. To test whether glutamate induces damage to hSOD1^{G93A} or ^{G85R}-expressing astrocytes through glutamate receptor-mediated signaling, we applied the amino acid in the presence of a mixture of glutamate receptor antagonists, the mGluR blocker (*S*)-α-methyl-4-carboxyphenylglycine (MCPG, 500 μM) and the AMPA/kainate receptor antagonist, 6-cyano-7-nitroquinoxaline-2,3-dione (CNQX, 10 μM; Figure 6b). This mixture completely prevented the glutamate toxicity.

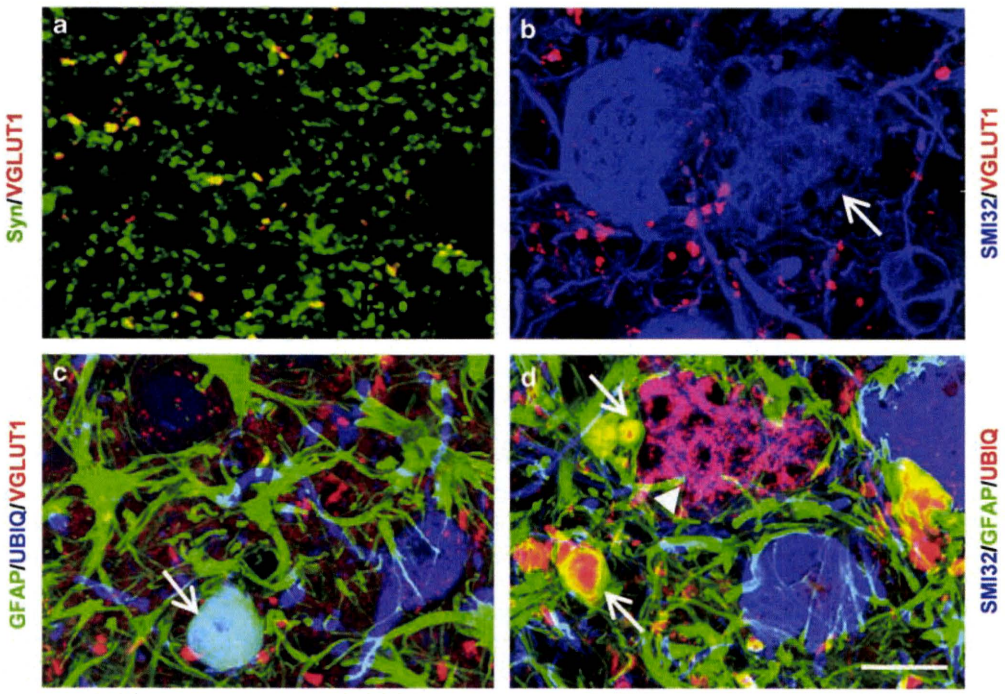

Figure 5 Degenerating astrocytes are surrounded by glutamatergic terminals immunolabeled for the vesicular glutamate transporter 1 (VGLUT1). (**a**) Representative image of spinal cord sections from hSOD1^{G93A} mice immunostained for synaptophysin (Syn) and VGLUT1. Note the massive colocalization of synaptophysin- and VGLUT1-positive puncta in the ventral horns. (**b**) Double immunostaining against SMI32 and VGLUT1 shows that VGLUT1-immunoreactive boutons end on motor neuron cell bodies and dendrites. Arrow indicates a suffering and vacuolated motor neuronal cell body. (**c** and **d**) Ubiquitin-positive SGPCs (arrows) are enclosed by glutamatergic presynaptic terminals (**c**) and they are located in the motor neuron microenvironment (**d**). Arrowhead indicates a ubiquitin-positive vacuolated motor neuron in (**d**). Scale bar, 20 μm (**a**–**d**)

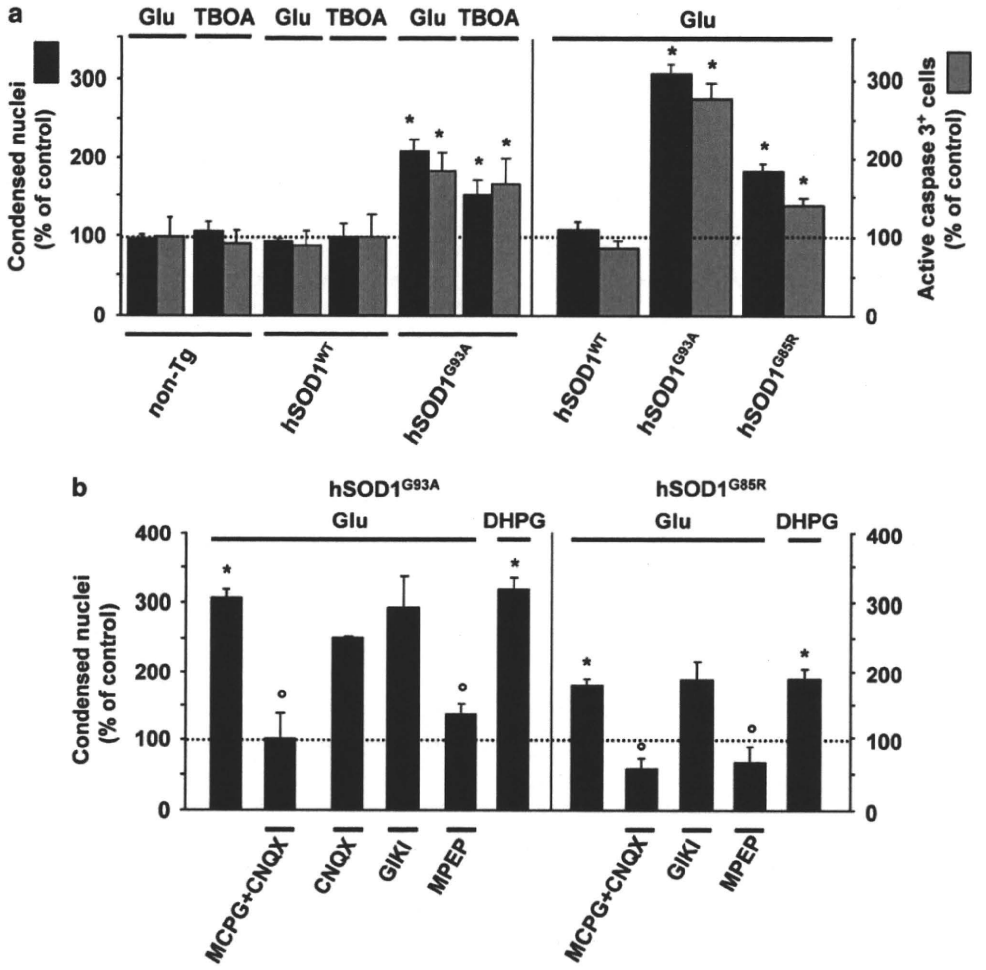

Figure 6 Expression of mutant hSOD1 confers glutamate vulnerability to spinal cord astrocytes through mGluR5-dependent signaling. (**a**) Left, a 30 min challenge with glutamate (500 μM) or the glutamate uptake inhibitor TBOA (200 μM) promotes within 24 h nuclear condensation (black bars) and caspase-3 activation (gray bars) in astrocyte cultures from $hSOD1^{G93A}$ mice, but not in those from nontransgenic (non-Tg) or $hSOD1^{WT}$ transgenic animals; ($n=3$ in triplicate). Data (mean ± S.E.M.) are expressed as percentage of control, that is, the corresponding culture type challenged with saline (cells with condensed nuclei: non-Tg: 1.2 ± 0.1%; $hSOD1^{WT}$: 1.3 ± 0.1%; $hSOD1^{G93A}$: 1.2 ± 0.1%; cells immunopositive for active caspase-3: non-Tg: 0.3 ± 0.1%; $hSOD1^{WT}$: 0.5 ± 0.1%; $hSOD1^{G93A}$: 0.3 ± 0.1%, respectively). Right, transfection with cDNAs encoding $hSOD1^{G93A}$ or $hSOD1^{G85R}$ mutants, but not $hSOD1^{WT}$, confers glutamate vulnerability to normal astrocytes from the rat spinal cord. Experimental paradigm and data expression are as in the left panel ($n=7$ in triplicate). Control values: cells with condensed nuclei: $hSOD1^{WT}$: 4.1 ± 0.4%; $hSOD1^{G93A}$: 3.5 ± 0.4%; $hSOD1^{G85R}$: 5.2 ± 0.5%; cells immunopositive for active caspase-3: $hSOD1^{WT}$: 6.5 ± 0.7%; $hSOD1^{G93A}$: 5.8 ± 0.7%; $hSOD1^{G85R}$: 7.4 ± 1.1%. (**b**) Glutamate-induced toxicity to mutant hSOD1-expressing astrocytes is selectively mediated by mGluR5 receptors. Rat spinal astrocytes transfected with either $hSOD1^{G93A}$-(left) or $hSOD1^{G85R}$-encoding (right) expression vectors were challenged with glutamate as above, in the absence ($n=7$ in triplicate) or in the presence of different glutamate receptor antagonists ($n=3$ per each condition), or with the group I mGluR agonist DHPG (100 μM; $n=4$ in triplicate). Data are expressed as percentage of control as above (*$P<0.05$ *versus* control (saline), °$P<0.05$ *versus* glutamate; ANOVA followed by Fischer PLSD method)

However, individual antagonists had different effects: CNQX, as well as GYKI 52466 (50 μM), an AMPA receptor-selective blocker, did not prevent glutamate toxicity, whereas 2-methyl-6-(phenylethynyl)-pyridine (MPEP, 200 nM), a selective mGluR5 antagonist, abolished it. Accordingly, (RS)-3,5-dihydroxyphenylglycine (DHPG, 100 μM), a selective group I mGluR agonist, fully reproduced the toxic effect of glutamate (Figure 6b). Altogether, these data reveal the specific role of mGlu5 receptors in mutant hSOD1-dependent astrocyte vulnerability.

***In vivo* administration of the mGluR5 antagonist MPEP slows down astrocyte degeneration, delays disease onset and extends survival.** On the basis of the above observations, we assessed the therapeutic efficacy of mGluR5 blockage *in vivo* in $hSOD1^{G93A}$ transgenic mice. Starting at the age of 40 days, animals were treated daily with MPEP (30 mg/kg intraperitoneally) or saline. Thereafter, mice were monitored daily for the first signs of hindlimb muscle weakness and weekly for the decline in body weight. Weight gain stops at the time of disease onset, and is followed by a steady decrease, which strictly correlates with the decline in motor performance.[7,8] Thus, the peak in the body weight curve is taken as a measure of the earliest onset of disease.[7,8] According to this criterion, as well as to the monitoring of hindlimb muscle weakness (not shown), we found that MPEP-treated mice showed a significant delay in the onset of the disease compared with controls (saline: